PNL-11463
UC-702

A Comprehensive Analysis of Contaminant Transport in the Vadose Zone Beneath Tank SX-109

A. L. Ward
G. W. Gee
M. D. White

February 1997

Prepared for the U.S. Department of Energy
under Contract DE-AC06-76RLO 1830

Pacific Northwest National Laboratory
Richland, Washington 99352

MASTER

DISCLAIMER

Portions of this document may be illegible in electronic image products. Images are produced from the best available original document.

Executive Summary

The Vadose Zone Characterization Project is currently investigating the subsurface distribution of gamma-emitting radionuclides in S and SX Waste Management Area (WMA-S-SX) located in the 200 West Area of the U.S. Department of Energy's Hanford Site in southeastern Washington State. Spectral-gamma logging of boreholes has detected elevated ^{137}Cs concentrations as deep as 38 m, a depth considered excessive based on the assumed geochemistry of ^{137}Cs in Hanford sediments. Routine groundwater sampling under the Resource Conservation and Recovery Act (RCRA) have also detected elevated levels of site-specific contaminants downgradient of WMA-S-SX. The objective of this report is to explore the processes controlling the migration of ^{137}Cs, ^{99}Tc, and NO_3^- through the vadose zone of WMA-S-SX, particularly beneath tank SX-109.

A series of hypothetical cases was simulated using STOMP, a multi-dimensional flow and transport simulator. The simulations represent the migration of contaminants from a region surrounding tank SX-109. Effects of varying recharge, specific gravity of the leaked fluid, distribution coefficients (K_ds), and varying complexity of sediment layering were simulated under known or assumed tank farm conditions from 1964 through the year 2015. Also considered were cases with and without preferential flow, and with and without a water line leak of 946 m^3 (250,000 gal) over a 75-day period. Fluid densities of 1.0, 1.4, and 1.65 Mg m^{-3} were simulated to evaluate the effect of wetting front instability. Leak volumes ranging from a 15 m^3 (4,000 gal) to 946 m^3 (250,000 gal) were simulated. Most of the simulations assumed a leak of 500 m^3 (132,000 gal). Imposed on the leaks was recharge of meteoric water (rain and snowmelt) at steady rates of 100, 10, and 0.5 mm yr^{-1}. In addition, a variable recharge rate, dependent on annual precipitation, was simulated. A range of K_ds was assumed for ^{137}Cs. Values ranged from 0 mL g^{-1}, chosen to reflect the effect of high salt concentration, pH, and high temperature on ^{137}Cs mobility, to 37 mL g^{-1}. A time-dependent K_d was selected to mimic the inverse dependence of sorption on Na^+ concentration. The K_d of ^{99}Tc and NO_3^- was fixed at 0 mL g^{-1}. All but two of the simulations were run for 51 years (1964 through 2015). Two of the simulations for ^{99}Tc and salt ($NaNO_3$) were run for several hundred years to look at peak concentrations of mobile contaminants at the water table.

The simulations illustrate the effect of key parameters on leak migration in vadose zone of WMA-S-SX tanks. Water flux past the base of the tanks ranged from three to five times the imposed flux because of tank shedding. Gravity fingering, resulting from fluid density contrasts, was demonstrated for the higher density fluids. Failure to include small-scale textural variations resulted in predominantly vertical transport and reduced travel times to the water table. When a sloped layer of coarse sand was incorporated in the model at a depth of 23 m, the simulated ^{137}Cs plumes showed peaks slightly above that depth, which was similar to most of the profiles observed in boreholes that had elevated ^{137}Cs. A K_d of 0 mL g^{-1} moved the ^{137}Cs unrealistically deep and into the water table, while K_ds of 0.5, 3, and 37 mL g^{-1} and various combinations kept ^{137}Cs from arriving at the water table in 50 yr, except under the most extreme conditions (high density, high recharge, preferential flow). A time-dependent sorption appeared to simulate more realistically the movement of ^{137}Cs than did assuming a constant K_d. An initially low K_d followed by gradually increasing values contained ^{137}Cs within a 40-m depth, with the center of mass at 21.3 m and a variance of 2 m^2 about the center of mass.

Recharge rates also had a profound effect on the contaminant migration. Under high recharge rates, ^{99}Tc and NO_3^- moved rapidly to the water table, arriving within 30 years of the initial leak. Reducing the recharge to 0.5 mm yr^{-1} prevented ^{99}Tc from arriving at the water table. Given the unavailability of site-specific data and the uncertainty in the contaminant release history, the simulations successfully reproduced the major features of observed contaminant migration in WMA-S-SX, including elevated ^{99}Tc concentrations in the groundwater as well as ^{137}Cs peaks and distributions in the vadose zone below the tanks. Simulations coupled with site data can be used to assess impacts from tank leaks and to evaluate mitigation strategies to prevent leaks. However, model calibration for the immobile contaminants will require more information than can be obtained from spectral-gamma logging of the vertical boreholes.

Acknowledgments

We thank K. M. (Mike) Thompson of the DOE for providing guidance, support, and management oversight of this work. Thanks also to C. T. Kincaid, M. D. Freshley, R. J. Serne, and V. G. Johnson for reviewing an earlier draft of this report.

Contents

Figures

Tables

1.0 Introduction

The U.S. Department of Energy, Richland Operations Office (DOE-RL) initiated a study in 1994 of subsurface contamination resulting mainly from past leaks of single-shelled tanks (SSTs) in 12 of the Hanford Site's 18 Tank farms. This Tank farm Vadose Zone Characterization Project (VZCP) is currently investigating the location and concentration in subsurface soils of gamma-emitting radionuclides such as cesium and cobalt, which can be detected by measuring their specific radioactive energies through existing steel-cased boreholes around each of the SSTs. The boreholes or so-called "drywells" extend to between 23 and 38 m (75 to 125 ft.) below the soil surface. Water table depth in the 12 tank farms varies from 64 to 76 m (210 to 250 ft.) below the surface.

The VZCP has been conducted for DOE-RL by the DOE-Grand Junction Projects Office (GJPO). Individual boreholes are logged with spectral-gamma analysis tools, and raw measurements are then analyzed and interpreted by the DOE-GJPO technical team. The borehole logging results for each SST are presented in individual Tank Summary Data Reports. When analysis of all tanks in a particular Tank farm have been completed, the results are then combined and discussed in a specific Tank farm Report. The first completed report is for the SX Tank farm (GJPO 1996).

Profiles of ^{137}Cs contamination beneath the SX-Tank farm are documented in the SX Tank farm summary report. Because of its generally assumed high distribution coefficient (K_d), ^{137}Cs is believed to have a low potential for migration. However, observed profiles suggest that ^{137}Cs contamination extends to depths of at least 38 m (125 ft.), and may extend even deeper. The current interpretation of depth and extent of contamination relies primarily on spectral-gamma surveys completed by the GJPO. However, supplemental information from past gross-gamma surveys also support the observation that ^{137}Cs contamination exists at the base of a number of the boreholes, particularly those that were deepened.

In addition to the presence of assumed immobile contaminants at greater-than-expected depths, there is also evidence of mobile species in the groundwater in the vicinity of the SST waste management area (WMA). Technetium-99, a mobile radioisotope forming a significant component of SST waste, exceeded the drinking water standard (DWS) of 900 pCi L^{-1} in 1993 but has declined to less than the DWS since 1994 (Caggiano et al. 1996). Chromium (as chromate) concentrations have also shown a time response similar to ^{99}Tc. Groundwater sampling has shown specific conductances in excess of the background value of 0.248 dS m^{-1} (248 μmho cm^{-1}). An increase in specific conductance in groundwater is often associated with increasing concentrations of mobile ionic species. Thus, the observation that groundwater concentrations of Ca^{2+}, Mg^{2+}, and Na^{+} increased with increasing NO_3^- and ^{99}Tc concentrations is not surprising. Flushing of Ca^{2+} and Mg^{2+} from sediment surfaces and subsequent replacement with Na^{+} is an expected chemical reaction (Caggiano et al. 1996).

Caggiano et al. (1996) presented several hypothetical sources, migration pathways, and driving forces that could have moved immobile contaminants such as ^{137}Cs to deeper-than-expected depths, and moved the mobile contaminants to the groundwater. The mechanisms and pathways are summarized in Figure 1.

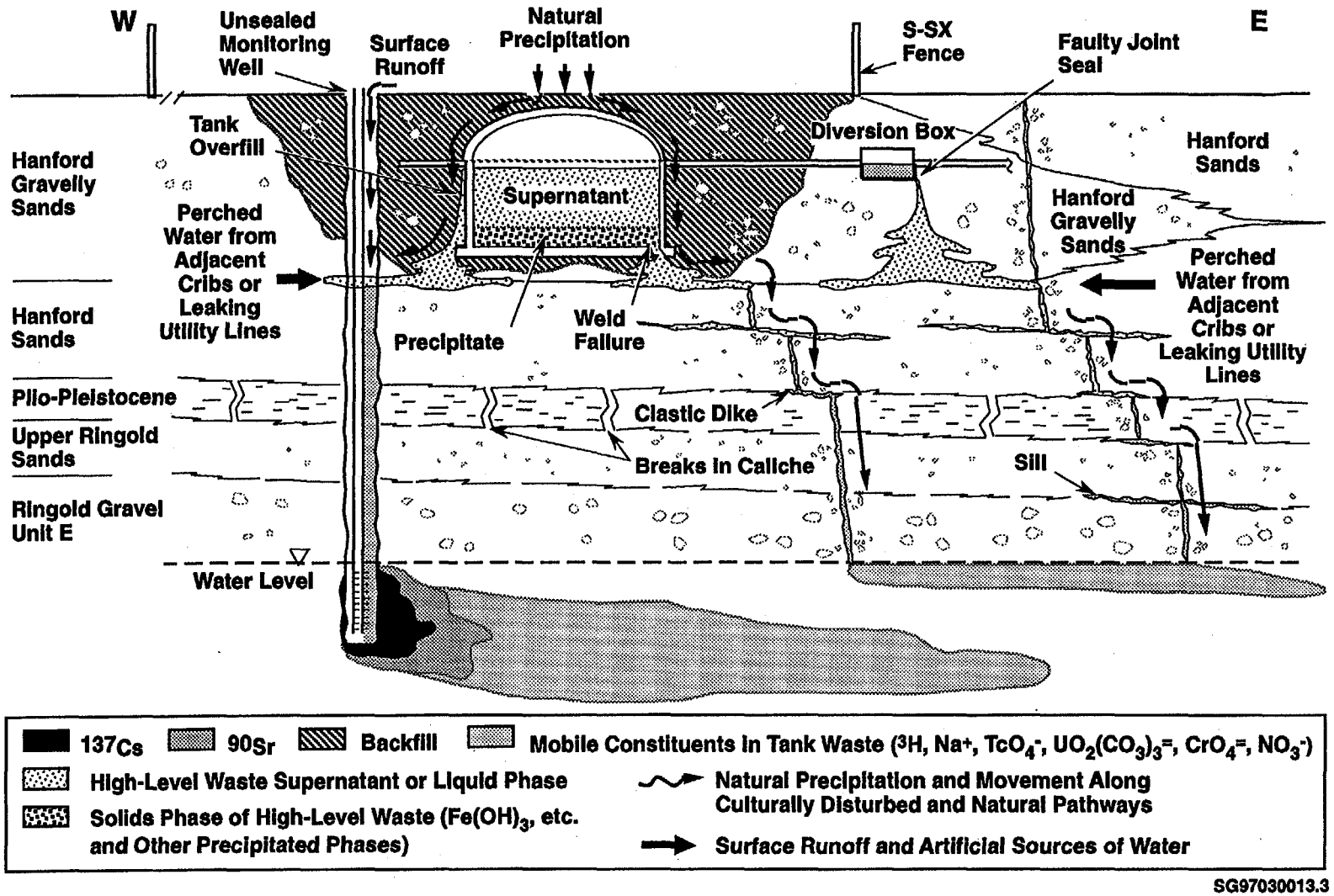

Figure 1. Hypothetical Sources and Potential Pathways Through the Vadose to the Groundwater at WMA-S-SX (after Caggiano et al. 1996).

What presently is unknown is the pathway by which ^{137}Cs reached the excessive depths observed at WMA-S-SX. Did the ^{137}Cs move throughout the entire subsoil, or did the tank leak intercept the drywell and move down the outside of the casing? Was the contamination in the deeper wells pushed there as the borehole was extended? Are there other explanations for the extent of the ^{137}Cs plume in the vadose zone?

Regardless of the driving force or migration pathway, the Resource Conservation and Recovery Act (RCRA) groundwater monitoring program suggests that wastes from the SSTs within WMA-S-SX have impacted groundwater quality. Furthermore, the Vadose Zone Characterization project (VZCP) show immobile species at significantly greater depths than would have been expected based on current belief about the geochemistry of these species. When coupled with the analysis of field observations, numerical modeling has the potential to test the importance of various mechanisms and refine the conceptual model hypothesized in Figure 1. Ultimately, modeling can help to evaluate the various proposed corrective measures by considering the relative importance of different pathways and contaminant-soil interactions.

While there have been numerous modeling studies conducted at the Hanford Site, not many have focused on the SSTs. Previous modeling studies of water flow, mass, and energy transport in the vadose zone include those of Arnett et al. (1977), Smoot et al. (1989), Smoot and Sagar (1990), and more recently Low et al. (1993), Piepho (1994), and Wood et al. (1996). Although these studies focused on different aspects of contaminant transport, their common link was the difficulty in calibration caused by a shortage of data specific to the sites of interest. Generalized information on soil stratification, moisture-dependent soil characteristics, and contaminant-soil interactions were used as input in the models. In general, uncertainty in the radionuclide inventories, tank leak volumes, leak rates and locations were also high. The current effort is aimed at modeling water flow and contaminant transport in the SX Tank farm, using a refined conceptual model with more realistic boundary conditions, hydrologic data, and chemical input data.

2.0 Scope and Objectives

The primary objective of this study is to explore the processes controlling contaminant migration in the vadose zone of the 241-SX tank farm. In order to accomplish this objective, several hypothetical flow and transport scenarios are simulated with a numerical model and the results are analyzed to determine the dominant processes. Since information concerning actual values of many input parameters is mostly lacking, a wide range of possibilities is examined to provide a range of possible outcomes. A parametric analysis is used to isolate the most critical parameters without the computational effort of a Monte Carlo simulation or the inflexibility of small perturbation methods. It is anticipated that the critical issues and parameters identified in this analysis will be studied further in order to provide the necessary guidance for laboratory and field investigations. It is also anticipated that this analysis will be useful in the evaluation of various corrective measures appropriate to WMA-S-SX, and other tank farms at the Hanford Site.

3.0 Modeling

Mathematical models employed to predict the fate of hazardous contaminants in variably saturated geologic media can be important tools for addressing problems of environmental management. Numerical models are useful for testing alternative conceptual models, selecting characterization strategies, explaining field observations, and subsequently evaluating corrective measures. However, it should be recognized that fluid flow and contaminant transport in natural systems is a complex problem that at present cannot be solved in its entirety. The successful application of a mathematical model is therefore dependent on an appropriate balance between the level of detail required and what is actually known about the system, and the availability of *good-quality, site- and contaminant-specific data.* A critical step in the modeling process is the development of a conceptual model that simplifies the problem while retaining the main processes occurring at the scale of interest.

3.1 Development of the Conceptual Model

3.1.1 The Mass Conservation Dilemma

Ten of 15 tanks at the SX-Tank farm have been identified as leakers. A summary of tank leak information supplied by Anderson (1990), Brevick et al. (1994), and GJPO (1996) is shown in Table 1. An estimate of 946 m^3 (250,000 gal) was assumed to represent the leakage volume from the SX-109 Tank. This is more than double the estimated 435 m^3 (115,000 gal) T-106 tank leak (Freeman-Pollard et al. 1994), which, until recently, has been cited as the largest tank leak at the Hanford Site (GAO 1989, Anderson 1990). Total leakage from the entire SX Tank farm is estimated to be slightly over 1.514 x 10^3 m^3 (400, 000 gal). As can be seen from Table 1, there is great uncertainty in tank leak volume estimates. Because of the uncertainty in the rates and times of liquid discharge, it is not known whether the observed distributions of contaminants in the soil and groundwater could have resulted from waste emanating from the SSTs.

Data from Raymond and Shdo (1966) show that the ^{137}Cs concentrations in the leaking fluids could range from 0.2 to 2 Ci L^{-1}. Assuming a worst case of 2 Ci L^{-1} in 946 m^3 (250,000 gal), the total ^{137}Cs inventory in the sediment would be 1.9 x 10^{18} pCi. Such large levels of contamination have yet to be documented by spectral-gamma logging but cannot be ruled out. An example of what has been documented is provided in the analysis of data from tank SX-109. In reviewing the data from this tank, it appears that the spectral-gamma logging in wells adjacent to tank SX-109 have only detected a small fraction of the total inventory. Using data from all boreholes surrounding tank SX-109, including the kriged 3D profiles of ^{137}Cs from the SX tank farm report (GJPO 1996), we calculate that less than 1/100 of one percent of the 1.9 x 10^{18} pCi inventory has been accounted for. Identifying where the rest of the inventory is located in the vadose zone is critical to a reliable analysis. Table 2 summarizes a simple analysis illustrating the expected concentrations at a monitoring drywell near the edge of the tank as a function of leak volume and time. The simplified calculations assume a sediment bulk density of 1.8 Mg m^{-3} and a uniform distribution within the soil profile for a leak that has spread over a 30-m diameter to a depth of 10 m below the bottom

Table 1. Current Status of SX Tanks in WMA-S-SX

Tank	Brevick (1995) Designation and Date of Leak	Drainable Liquid in Tank Today[(a)] (gal)	Anderson (1990) Estimated Leak[(a)] (gal)	GJPO (1996) Estimated Leak[(a)] (gal)
SX-101	sound	146,000	0	
SX-102	sound	183,000	0	0
SX-103	sound	223,000	0	0
SX-104	leak, 1988	201,000	0	5,300
SX-105	sound	261,000	0	0
SX-106	sound	233,000	0	0
SX-107	leak, 1964	0	<500	5,000
SX-108	leak, 1962	0	2,400	35,000
SX-109	leak, 1965	0	<500	250,000
SX-110	leak, 1976	0	0	5,300
SX-111	leak, 1974	0	2,000	2,000
SX-112	leak, 1969	0	30,000	30,000
SX-113	leak, 1962	0	15,000	15,000
SX-114	leak, 1972	0	0	8,000
SX-115	leak, 1965	0	50,000	50,000
Totals		1,247,000	100,400	405,600

(a) To convert gallons to liters, multiply by 3.785 L/gal.

Table 2. Calculated Borehole Concentrations as a Function of Leak Volume and Time

Leak Volume (gal)	Curie Load (pCi)	Soil Mass Affected (Mg)	Drywell Conc. (pCi/g) in 30 yr	Drywell Conc. (pCi/g) in 300 yr	Drywell Conc. (pCi/g) in 1000 yr
1.0×10^{4}	7.57×10^{16}	1.27×10^{4}	2.97×10^{6}	5.79×10^{3}	6.89×10^{-4}
1.32×10^{5}	1.00×10^{18}	1.27×10^{4}	3.92×10^{7}	7.46×10^{4}	9.09×10^{-3}
2.5×10^{5}	1.89×10^{18}	1.27×10^{4}	7.43×10^{7}	1.86×10^{5}	1.72×10^{-2}

of the tank. To simplify the calculations, it is assumed that the contaminant is fixed in space after 30 yr, and that a perfect cover exists so that recharge and internal drainage cease at that time.

This analysis indicates that very high concentrations of contaminants could persist for up to 10 half-lives (300 yr) in the boreholes. These calculations illustrate that if a perfect cover is placed over the tanks and movement ceases, even after 300 yr the boreholes will still indicate measurable amounts of ^{137}Cs. Only after 1000 yr will levels of ^{137}Cs fall below detection limits. Realistically, the shape of the distri-pbutions and the time course of the measured concentrations should show transient behavior and respond to continued leaching from infiltrating rain and snowmelt events. Also if preferential flow paths exist under the tanks and after 30 yr the K_d remain low, then the concentrations would be less than those reported. It is clear however, that accounting for the leak volume and keeping track of the mass balance using spectral-gamma logging has severe limitations.

Sampling in accordance with the requirements of the RCRA groundwater monitoring plan shows that several site-specific constituents have exceeded the DWS. In particular, concentrations of ^{99}Tc down-gradient of the SX Tank farm exceeded the 900 pCi L^{-1} DWS in 1993. Records of other mobile species such as NO_3^-, Na^+, Ca^{2+}, Mg^{2+}, and CrO_4^{2-}, as well as changes in the specific conductance, show a similar trend (Caggiano et al. 1996). With respect to the less mobile gamma-emitting species, spectral-gamma logging of the boreholes in the SX Tank farm shows that the zone between tanks SX-109 and SX-112 contains the highest ^{137}Cs concentration of all 96 drywells in the SX Tank farm, at depths exceeding 38 m (125 ft.) (GJPO 1996). There is also evidence from gross-gamma logging that tank SX-109 was leaking as recently as 1992 at rates and amounts that are presently undetermined. These observations have raised several questions about transport of ^{137}Cs in the vadose zone. Given the K_d generally assumed for ^{137}Cs, it has often been suggested that this contaminant has a low potential for migration, especially under the low recharge rates usually assumed for Hanford.

Certain characteristics about the rate of migration of ^{137}Cs in Hanford sediments can be easily demonstrated by revisiting the data from Raymond and Shdo (1966) and comparing them with the more recent data reported by GJPO (1996). Raymond and Shdo (1966) reported on a study undertaken to characterize the spread of contamination below tanks SX-115 and SX-108 as a basis for determining the extent of tank leakage that occurred in 1962. The distribution of ^{137}Cs was determined by quantitative analysis of gamma spectra from soil cores in early 1965. Data from the SX-108 evaluation showed two superimposed leak zones near the north, north west section of the tank. An analysis of the moments of the resident probability density function (Appendix A) shows that in the vicinity of the leak (near present-day well W41-08-11), the bulk of the ^{137}Cs was located between 13.7 m (45 ft.) and 20.7 m (68 ft.) below the surface, with a peak concentration of around 1×10^8 pCi g^{-1} at a depth of 16.7 m (55 ft.). The center of mass was located at 17.25 m (56.59 ft.), and the distribution had a variance of 0.78 m^2 (8.44 $ft.^2$). These data dispute a widely accepted belief about ^{137}Cs migration in Hanford sediments. The migration of ^{137}Cs to a depth of 16.7 m in less than 3 yr suggests that in the chemical environment associated with wastes from the reduction-oxidation (REDOX) process, the assumption of a K_d much greater than zero cannot be justified.

More recently, spectral-gamma logging conducted by GJPO in June 1995 could determine neither the peak concentration nor its location on well W41-08-11. However, the data show the bulk of ^{137}Cs between 13.7 m (45 ft.) and 22.9 m (75 ft.). No data were collected between 14.8 m (48.5 ft.) and 19 m (62.5 ft.),

where saturation of the detector of the logging instrument occurred. Nevertheless, assuming a normally distributed resident concentration profile, a weighted least-squares analysis located the peak at 17 m (56 ft). Between 1965 and 1995, it appears that the peak moved less than 0.5 m (1.6 ft.). The greatest change in ^{137}Cs concentration occurred between 19.8 m (65 ft.) and 20.9 m (75 ft.). The concentration increased from 1 pCi g^{-1} to about 5 pCi g^{-1}, suggesting a very slow migration of the leading edge of the plume. Without a complete distribution, it is difficult to accurately determine transport the characteristics. When coupled with the data from Raymond and Shdo (1966), these data suggest that in the period immediately following a leak, the K_d of ^{137}Cs is near 0 mL g^{-1} but eventually increases to a higher, but presently undetermined, value. The increase in K_d, coupled with a favorable soil-textural sequence, could severely limit any further migration.

Figure 2 summarizes the gross gamma surveillance logs from borehole 41-09-09 for the period 1975 through 1994 . In 1975, a single peak was observed at 19.5 m (64 ft.), as shown in Figure 2a. In 1982, the intensity started to increase at the 22.5 m (74 ft.) depth showing a sharp increase in rate in 1986 and again in early 1988 (Figure 2b). This led to the development of a bimodal distribution, with the highest concentration occurring at 22 m (73.5 ft.) below ground surface, while a peak of lower intensity occurs at 19.5 m (66 ft.). This profile contains information critical to the development of the conceptual model. Immediately following a leak, sorbing gamma emitters such as ^{137}Cs would have moved quickly through the first few meters of soil because of the near-zero K_d caused by the high concentration of competing cations. When combined with the large leak volume and the low capillarity of the Hanford Sand Unit, migration would have been predominantly vertical. The smaller peak at 19.5 m (64 ft.) suggests the presence of a layer of somewhat coarser texture and higher hydraulic conductivity than the surrounding Hanford Sand unit. However, the transport properties did not permit the contaminant to come close enough to the borehole to show up as a high concentration, hence the lower peak count rate. At 20.9 m (68.5 ft.), the count rate dropped back to a level slightly higher than in the soil above the coarse-textured lens. This observation sets bounds on the thickness of the coarse lens to around 1 m. The higher peak at 22 m (72 ft.) suggests the presence of another coarse layer that is much thicker than the one at 19.5 m (64 ft.), and with hydraulic and transport properties that allowed more of the contaminant to move toward the borehole as of 1982.

Integration of the count rate, C, over depth, z, gives an indication of the total mass of gamma-emitting radionuclides detected by probe from within the borehole. Assuming no further leaks or outside sources, $\int C(z)\, dz$, should remain constant, or decrease in response to radioactive decay. The increase in $\int C(z)\, dz$ with time, as shown in Figure 2b, could be indicative of either a renewed source of contaminant, or remobilization of the existing plume. The fact that the increasing intensity is limited to the 22 m (72 ft.) depth suggests a hydrologic limitation to movement such as contrasting hydraulic properties (e.g., a capillary break) and an insufficient hydraulic gradient to overcome them. Such an occurrence would result in an apparent increase in concentration detected from inside the borehole as the plume approaches the borehole. The preceding argument establishes a strong link between the movement of gamma emitters and stratigraphy, a link that is developed further in the next section. Since these data reflect the impact of all gamma emitters, it is unknown whether the changes are due to mobile or sorbing species. If, due to a sorbing species, these results would suggest either the replacement of the sorbed species or movement under conditions of near zero K_d. Either scenario would require a renewed leak from the tank.

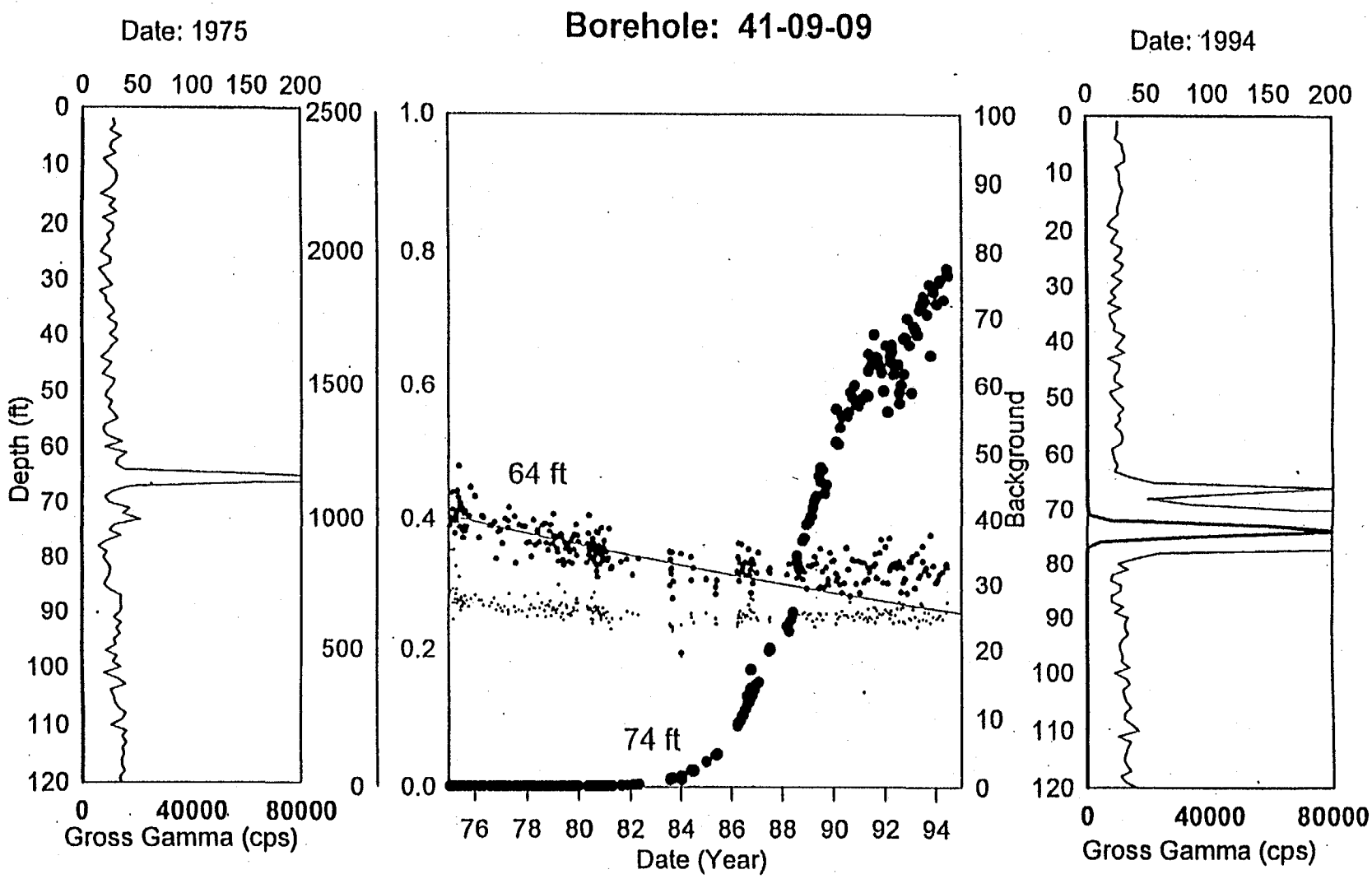

Figure 2. Analysis of Borehole Logs for Borehole 41-09-09 Showing (a) Gross Gamma-Ray Intensity Versus Depth in 1975, (b) Integral of Gamma-Ray Intensity Over Depth at 22 m Versus Time, and (c) Gross Gamma-Ray Intensity Versus Depth in 1994 (after Price 1996).

3.1.2 Stratigraphy

During the drilling of 96 boreholes and 6 water wells in and around the 241-SX tank farm, sediment samples were collected from 0.3 to 1.5 m (1 to 5 ft.) depth intervals and analyzed. The resulting data were used to prepare a series of maps depicting the geology underlying 241-SX tank farm (Price and Fecht 1976, Lindsey, 1991). The SX tank farm is underlain by four major stratigraphic units: (1) basalt of the Columbia River Group, which forms the bedrock beneath the farm; (2) semi-consolidated sediments of the Ringold Formation, which directly overlie the bedrock; (3) unconsolidated eolian silt; and (4) unconsolidated sand, silt, and gravel collectively known as glaciofluvial sediments, which directly overlie the eolian silt. The water table is presently at 64 to 66 m below ground surface. Figure 3 shows a cross-sectional view of the stratigraphy in a transect through tanks SX-108 and SX-109. The solid lines are contacts between lithologies, where accurately known. The dashed lines are approximate contact locations, while a queried dashed line is an inferred contact (Price and Fecht 1976). Discontinuous sediments, less than 0.6 m thick, are shown by short dashed lines, while those greater than 0.6 m are represented by a dashed polygon.

Several studies have shown that in naturally occurring systems, spatial variability in soil properties can result in complex three-dimensional flow paths, which may enhance solute dispersion. Funneling, due to textural discontinuities between layers of different hydraulic conductivities and inclined bedding planes, has been shown to increase solute velocity by 10 to 100 times (Kung 1989). More recent studies of transport of Cl^- in a layered, coarse-textured soil indicated that the horizontal spatial scale dependence of transport and solute recovery was related to the horizon thickness variability (van Wesenbeeck and Kachanoski 1994, Ward et al. 1995). Thus, the traditional approach of modeling of transport in layered soils with the advective-dispersive equation (ADE), assuming gross stratigraphic difference and constant horizon thickness (Smoot et al. 1989, Piepho 1994) may not be appropriate, since they may not properly capture the hydrologic control features of the lithology.

Aside from the four main stratigraphic units, the soil profile is characterized by numerous lenses ($\leq$ 0.6 m [2 ft.] thick). These lenses are generally of a finer texture than the surrounding host material. One lens of particular interest is a silty fine to very fine sand layer at a depth of 20 m (65.6 ft.) below ground surface, to the left of tank SX-109 (Figure 3). This lens is underlain by a slightly pebbly very coarse to coarse sand lens at a depth of 22 m (72 ft.) below the surface and close to a sloped lithologic contact. Recent gross-gamma ray intensities (Figure 2) show peaks attributed to ^{137}Cs at depths of 19.5 and 22 m (64 and 72 ft.) below the surface in the Hanford fine unit. These data, and data from the laterals below the tanks, suggest that contaminant migration in the vicinity of tank SX-109 was primarily vertical between 0 and 3 m (0 and 10 ft.) below the tank, and horizontal between 3 and 8.5 m (10 and 28 ft.) below the tank. The extent of lateral migration was greater in the 7 to 8.5 m (23 to 28 ft.) zone beneath the tank (Figure 2a). Such an observation suggests a strong link between contaminant distribution and small-scale stratigraphic variations in the vicinity of tank SX-109. The relationship between the small-scale variations in soil texture and the observed distribution of ^{137}Cs was investigated by closely examining neutron logs from the boreholes in the SX tank farm.

Neutron logs are commonly used to determine volumetric soil water contents, θ, provided the probe is calibrated and a relationship between count rate and θ exists. Without calibration, neutron logs can still

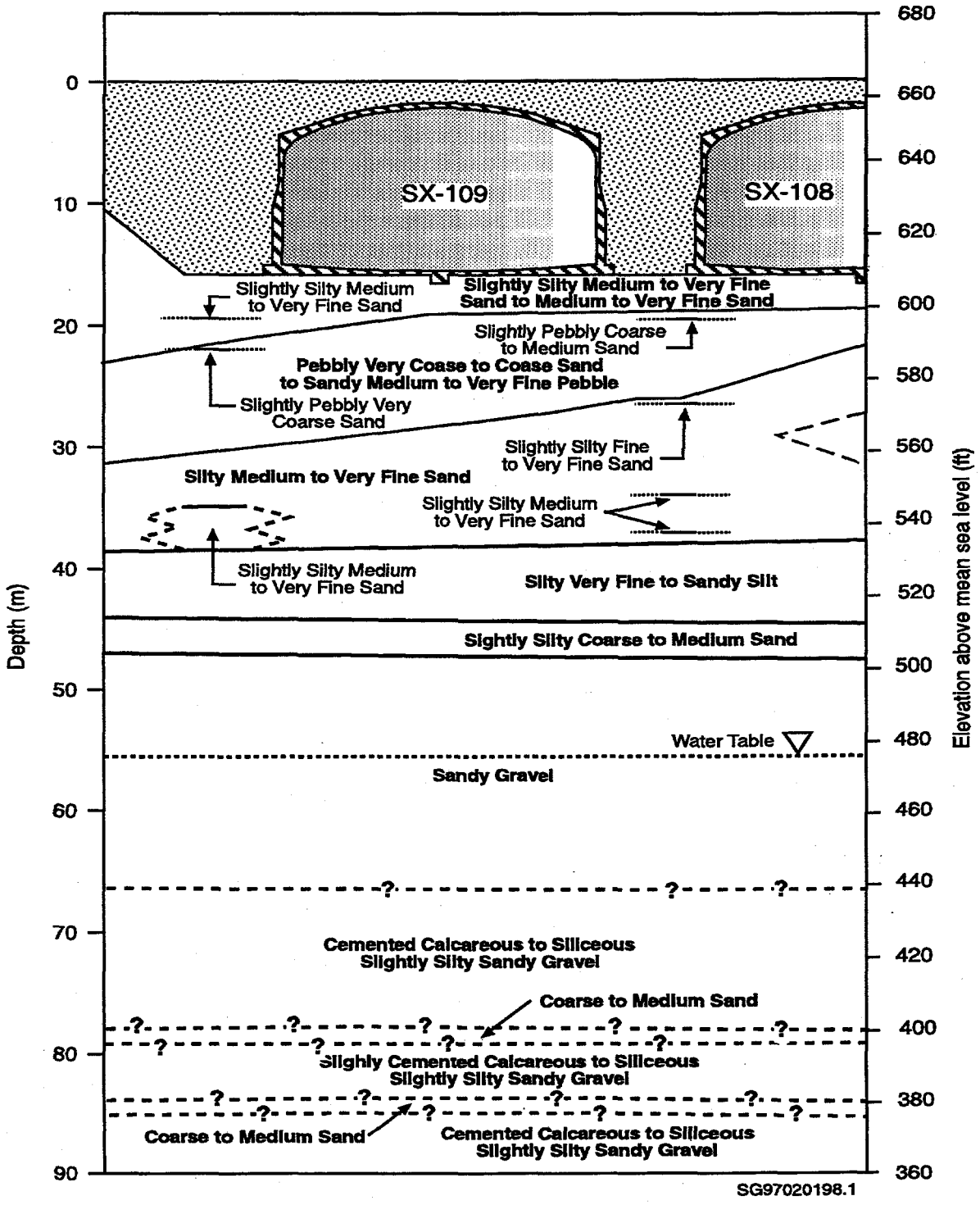

Figure 3. Geologic Characterization of SX Farm. The Cross Section Was Taken Through Tanks SX-108 and SX-109 (after Price and Fecht 1976).

provide useful information about the location of wetting fronts and relative changes in water content, and can be useful indicators of stratigraphic variation. In general, coarse-textured soils produce lower neutron counts than soils of a finer texture. The neutron logs from the SX tank farm were used in combination with descriptive logs obtained during well construction (Figure 3) and field observations of ^{137}Cs distributions (Figure 2) to refine the stratigraphic conceptual model. Figure 4 shows neutron logs from four wells to the north, south, east, and west of tank SX-109. Potential lateral flow pathways are indicated by the arrows. These zones represent soil layers that are coarser in texture than those immediately above and below them. During near-saturated flow events, such as would occur in response to a tank leak, transport velocities in these zones would be much higher than in the zones above and below them, leading to preferential lateral movement. Even in unsaturated flow conditions, transport velocities would be higher because of the smaller amount of pore water to displace. In the four wells shown in Figure 4, there are clearly defined coarse layers corresponding to those hypothesized in the previous section after analysis of the data in Figure 2a.

3.1.3 Precipitation and Recharge

Precipitation, in the form of rain and snow, was considered to be the major water source term in developing the conceptual model. The Hanford Meteorological Station (HMS) is located 5 km (3 mi) away from the SX tank farm, and maintains a database of climatic data that was used in the conceptual model. Thus, precipitation data proved to be the least uncertain of all the data required for simulating the tank leak. In order to reduce the complexity of the simulation, it was assumed that there was no water loss by surface runoff. Thus, surface infiltration was equal to precipitation. Even though precipitation is highly variable, an annual average value was chosen for some of the simulations. The long-term annual average precipitation for the site is more than 160 mm yr^{-1}. During the past 20 years, however, precipitation has averaged nearly 190 mm yr^{-1}, with the past two years reaching record values of over 300 mm yr^{-1} (Hoitink and Burke 1996).

Studies conducted over the last decade at Hanford suggest that recharge rates can vary from less than 0.1 mm yr^{-1} on a variety of soil and vegetative combinations to greater than 130 mm yr^{-1} on bare basalt outcrops or bare, gravel-surfaced waste sites (Gee et al. 1992). More recent data from experimental sites, including the Field Lysimeter Test Facility (FLTF) and the Prototype Hanford Barrier (PSB), both in the 200 Area, suggest that recharge through gravels can vary between 15 % and 70 % of precipitation, with the lower amount occurring under vegetated conditions (Gee et al. 1996, Fayer and Walters 1995, Fayer et al. 1996). The higher percentage translates into a recharge rate of 100 mm yr^{-1} and was observed on clean gravels that were free of vegetation. Drainage from bare sands is about 70 mm yr^{-1} under Hanford climatic conditions. However, there has been no measurement of recharge on tank-farm gravels, which are known to contain a larger amount of fines than the clean gravels discussed above. Thus, it is entirely possible that the tank farms may experience a recharge rate that ranges between that observed for bare sand and gravels at Hanford. More accurate estimates of recharge could be determined, by a water balance approach, as the difference between infiltration and water storage. Water storage could be determined easily by integrating depth profiles of water content. However, the absence of a calibration relationship for the neutron moisture logs prevents using the data presented in Figure 4 in this capacity.

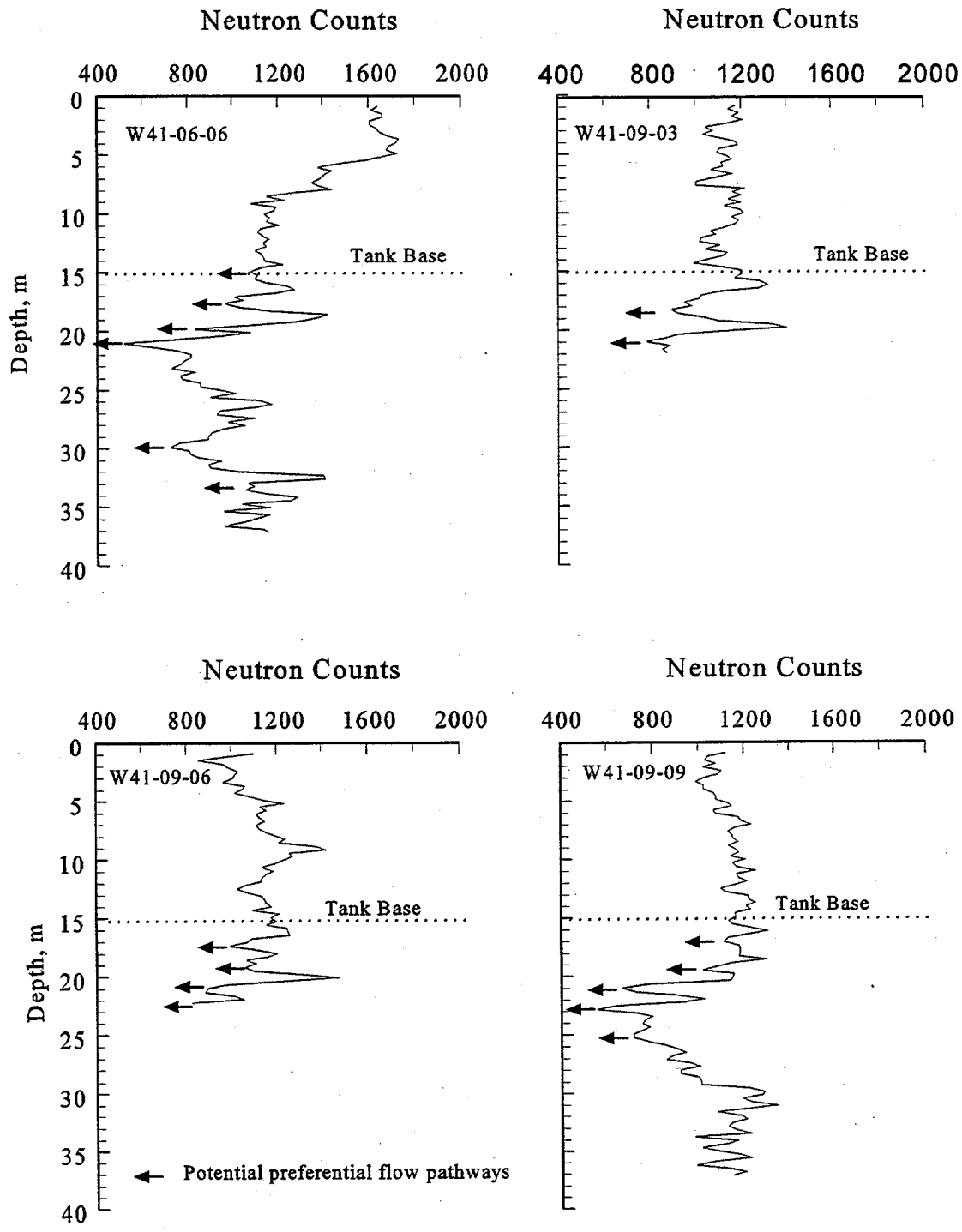

Figure 4. Neutron Logs of Four Boreholes Adjacent to Tank SX-109. Potential Lateral Preferential Flow Paths are Denoted by Arrows.

The uncertainty in recharge in a tank farm is increased further when the high heat load of most tanks is considered. High heat loads could further reduce the net infiltration, resulting in a reduced recharge. The current conceptual model does not account for thermal effect, which could cause drying, and possibly, even lower recharge rates. Heat generated in the tank could produce steam and subsequently cause drying around the tanks, especially during the initial tank filling and for some time thereafter (through the early 1970s). High temperatures could also promote wetting front instability, due to its influence on viscosity. If the thermal regime around the tank were better known, these effects could be more thoroughly analyzed. In order to capture the influence of variable recharge, as might have been caused by the effects of high heat loads, without introducing thermal effects and water flow in the vapor phase into the conceptual model, the recharge was limited to 6 % of precipitation for the period 1964 to 1983 and 40 % of annual precipitation thereafter. This assumption limited recharge to 10 mm yr^{-1} for 1964 through 1983. Strategies that control recharge, such as surface barriers, have been proposed as a means of limiting contaminant migration in the tank farms. A prototype Hanford barrier has been designed and built in the 200 W Area to limit recharge to $\leq$ 0.5 m yr^{-1} (Wing and Gee 1994). Thus, the impact of a permanent isolation surface barrier that would limit recharge to 0.5 m yr^{-1} was also considered in the conceptual model.

3.1.4 Soil-Contaminant Interactions

The mobility of radionuclides in the soil system depends on the physical and chemical properties of the soil, the chemistry of the soil solution, and the characteristics of the radionuclide and of the waste itself (Gee et al. 1983). Serne and Burke (1997) provides a summary of what is known about geochemical interactions between tank solutions and Hanford Sediments. Past simulations of tank leaks usually assumed a constant K_d of 100 mL g^{-1} for ^{137}Cs. There is a preponderance of evidence to suggest that such an assumption is invalid. Apart from the evidence obtained by revisiting the data of Raymond and Shdo (1966), there is also evidence in the scientific literature that lends support (Relyea and Silva 1981, Saiers and Hornberger 1996, Fujikawa and Fukui 1991).

Relyea and Silva (1981) showed both theoretically, with a double-layer model, and experimentally that the K_d of ^{137}Cs can vary from 10 mLg^{-1} to more than 10^3 mL g^{-1} as the concentration of NaCl decreased from 1 M to 0.01 M. Since these observations were made on a Belle Fourche montmorillonite clay, the applicability to Hanford coarse-grained sediments can be easily questioned. A recent study of ^{137}Cs migration through columns of quartz sand reported a similar result. Saiers and Hornberger (1996) found that the ability of mineral grains to adsorb ^{137}Cs decreased linearly with the log of the ionic strength of the conducting fluid containing Na^+. Fujikawa and Fukui (1991) reported a similar result. As in the study reported by Relyea and Silva (1981), the ionic strengths of interest were low (0.002 M to 0.1 M) compared to the ionic strengths of REDOX wastes. However, extrapolation of the reported studies clearly indicate that in the supersaturated solutions commonly comprising tank wastes, the K_d of ^{137}Cs would be initially near zero, but would gradually increase as the waste was diluted by infiltrating and antecedent pore waters. The K_d would eventually reach a value similar to that measured in laboratory batch experiments. In a recent study, Serne and Burke (1997) conducted a series of sorption experiments with simulated REDOX wastes. The results of this study show that in such a chemical environment, the K_d of ^{137}Cs ranges between 20 to 37 mL g^{-1}, some 3 to 5 times less than the lowest K_d assumed in previous modeling efforts at Hanford.

There are currently no data that describe the interaction between liquors from specific tanks in the SX tank farm and the different types of sediments. There are also no data that relate the variation in the K_d of ^{137}Cs with ionic strength in the range of values unique to Hanford wastes. Nevertheless, a number of assumptions were made in order to extrapolate what is known into the conceptual model. The logic of this extrapolation follows. It is known that the temperature of REDOX wastes from self-concentrating tanks was extremely high in the years immediately after the tanks were filled. The pH of the wastes was also quite high, as was the concentration of Na^+. Thus, to represent a hot caustic solution leaking from the tank, the K_d was assumed to vary between 0 and 0.5 mL g^{-1} in the first 8 yr of the tank leak. As the solution moved through the vadose zone, cooled, and the concentration of Na^+ decreased through dilution with meteoric and pore water, the K_d was assumed to increase to values ranging from 3.0 to 37 mL g^{-1}.

Dilution with both antecedent and advecting recharge waters, combined with decay, are hypothesized to have kept ^{137}Cs in the sediments well above the water table. The observation that no ^{137}Cs has been detected in downgradient wells of the SX tank farm qualitatively supports this hypothesis. It also implies that the velocity of ^{137}Cs would be more than 120 to 4000 times slower than the groundwater velocity. The relatively short half-life of ^{137}Cs, coupled with its retardation, should prevent significant mobility. Even if ^{137}Cs reached the groundwater, the expected travel distance for a time of 10 half-lives (302 years), assuming piston flow, would be less than 10 m at a groundwater flow rate of 0.3 m day^{-1}, which is the rate typical for this part of the Hanford Site.

3.1.5 Other Simplifying Assumptions

In reality, water flow and contaminant transport in the vadose zone may take place in three spatial dimensions. To simplify the simulation of reactive and decaying solutes through an unsaturated, layered soil profile, we considered a vertical slice of the flow domain and thus considered only a two-dimensional domain in the *xz* plane. A two-dimensional sectional approximation, however, can be considered conservative in the sense that predicted water contents and contaminant concentrations will always be greater than actual field values.

Caggiano et al. (1996) hypothesized that a water line leak could have contributed to the rapid migration of mobile and immobile contaminants to the groundwater. To date, there is no evidence of a water line leak occurring within the SX tank farm. However, recent events suggest that corroded cast iron utility water lines could produce a large volume of water over a very short time. In the conceptual model, we did not explicitly consider a water line leak, but by investigating the effect of an extreme recharge (100 mm yr^{-1}), the effects of such a leak can be qualitatively captured. As hypothesized in Figure 1, the movement of contaminants along preferential pathways such as clastic dikes, or unsealed monitoring wells, is another possibility. The probability of a tank encountering a clastic dike is substantial (Caggiano et al. 1996). However, information on clastic dikes and their hydrologic properties at Hanford is more or less qualitative rather than quantitative. Modeling of the effects of a clastic dike then becomes somewhat subjective. The same can be said about attempting to model other hypothesized preferential flow paths. While preferential flow pathways have been shown to be important in the movement of water and solutes in the field, there is still much to be understood about the dynamics of these pathways and how to model their effects. The enhanced transport of radionuclides facilitated by colloids in a salinity gradient (Fauré et al. 1996) was not considered in this study.

The injection of a hot liquid into initially cool porous media partially saturated with water is known to cause wetting front instability through the temperature dependence of the viscosity. This effect was not considered in the present conceptual model. Other processes such as soil water uptake by plants, offsite sources of recharge, flow of water in the vapor phase, and thermal effects were neglected. This assessment does not attempt to capture the complex interaction of potential dissolution of minerals and subsequent supersaturation or formation of gel-like materials that can subsequently precipitate and then redissolve over time. Although such processes could be expected to influence the soil hydraulic properties of the porous media, they were not considered in this study.

3.1.6 Conceptual Model

The region of interest in this study was the cross section through tanks SX-107, SX-108, and SX-109. Of particular interest was the western end of the cross section in which borehole 41-09-09 is located. Figure 5 shows a schematic of the grid used to discretize the simulation domain. The simulation domain extended 64 m (210 ft.) horizontally, and to a depth of 80 m (262.5 ft.). The water table was assumed to be located at a depth of 64 m (210ft.). The simulation domain was discretized into 36 cells horizontally and 85 cells vertically, using a variable grid spacing. Five major stratigraphic units were considered for this simulation. The top-most unit is a backfill material consisting of silty sandy gravel and extending down to 16 m (52.5 ft.) below the surface. The backfill material is underlain by a 24-m thick (79-ft. thick) layer of fine sand (Hanford fine sand unit). Below the Hanford sand unit is a 5 m-thick (16-ft. thick) layer of Early Palouse soil that overlays the 3-m thick (10-ft. thick) layer of gravel (Upper Ringold unit). Below this is a 32-m thick (105-ft. thick) layer of the Middle Ringold unit. At the scale of this simulation, it was assumed that the units were continuous, but not of constant thickness. Sloped interfaces were included where observed, and layers less than 0.6 m (2 ft.) thick were also included. The smallest cells (0.2 m x 1.0 m, [0.7 ft. x 3 ft.]) were located in the thin lenses and at the interface between the different textural units. The simulation domain encompasses a volume 1.23×10^3 m^3 (4.34×10^6 ft.^{3}) with a total of 3060 nodes. While location of the tank leak can have a significant impact of the simulation result, there is very little information to permit an objective choice. In this study, the leak was assumed to have occurred over a 12 m (39 ft.) distance (50 % of the tank diameter) as shown in Figure 5.

Unlike previous tank leak simulations, there is no detailed chronology of events associated with the SX-109 tank leak. Thus, the present scope is meant only to illustrate the relative importance of stratigraphic detail, leak volumes, recharge rate, and chemical interactions on contaminant migration. Because some aspects of the conceptual model preclude any detailed comparison with field data, some degree of caution is needed when comparing data from WMA-S-SX with the results of this study. There are many reasons why an exact match between simulated and measured data should not be expected. First, none of the input parameters (leak location, volume, rates, recharge rates, K_ds, or hydraulic properties) are known with any great degree of certainty. Second, spectral-gamma measurements in the vadose zone have detected ^{137}Cs as the principal contaminant. However, the more mobile contaminants (NO_3^- and ^{99}Tc) cannot be measured with gamma logging, so they have not been measured in the vadose zone. The information on ^{99}Tc and NO_3^- are available only from groundwater sample analysis. Third, some of the ^{137}Cs measurements may be have biased by borehole effects. There is evidence of gamma contamination internal and external to the borehole on at least two of the wells. Contamination has been found inside the borehole (41-12-02), and there are logging notes suggesting that gamma contamination was pushed down

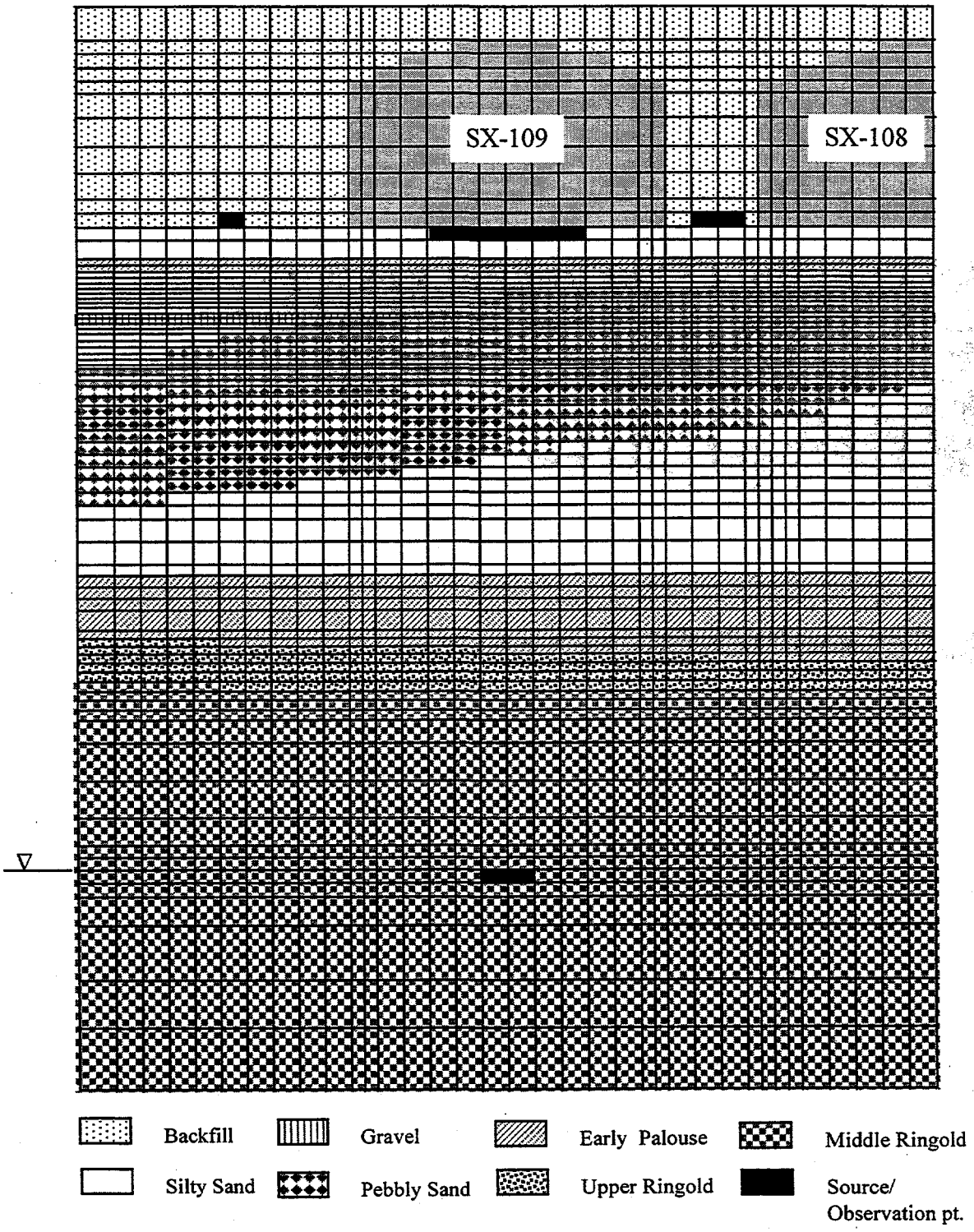

Figure 5. Schematic of the Two-dimensional Simulation Domain Showing the Major Stratigraphic Units Considered and the Location of the Source and Observation Points.

the outside of the casing when this hole was extended from 23 m (75 ft.) to 38 m (125 ft.) (GJPO 1996). Similarly, borehole 41-09-04 shows internal contamination and logging records suggest that contamination was also pushed down the outside of the casing when the borehole was extended from 23 m (75 ft.) to 36 m (110 ft.). The extent of the influence of borehole effects on the estimated ^{137}Cs concentrations is not known at present, but is under investigation.

3.1.7 Mathematical Model

Given the stratigraphic nature of the soil profile, it was determined that a multidimensional model capable of simulating water flow and transport of salt brines, as well as radioactive isotopes undergoing sorption and decay, would be most appropriate. The engineering simulator STOMP (Subsurface Transport over Multiple Phases) was modeled to solve the flow and transport problem. STOMP was developed for application to DOE problems under the volatile organic compounds (VOC) Arid demonstration project. STOMP is based on the numerical solution of the three-dimensional Richard's water flow equation and the advective dispersive equation for contaminant transport. The model is an integral-volume, finite difference simulator designed to solve a wide variety of multi-dimensional, nonlinear, and multi-phase, flow and transport problems in variably saturated geologic media (White and Oostrom 1996). The current version of the STOMP simulator is limited to Cartesian, tilted Cartesian, and cylindrical coordinate systems and can simulate six coupled flow equation combinations. All boundary conditions, sources, and sinks are time-variant allowing considerable control over transient simulations. Hydrologic properties can be spatially varied throughout the simulation domain within the resolution of node volume. The simulator also allows the use of anisotropic hydraulic, thermal, and transport properties for the porous medium. STOMP is capable of simulating flow and transport under isothermal or nonisothermal conditions. Transport of salt brines, as well as radioactive solutes with chain decay tracking, can be incorporated into all transport solutions.

3.2 Model Input Parameters

The quality of the results obtained from numerical simulations depends on the quality of the available input data. Unfortunately, there are very few site-specific hydraulic and transport data available for the region of interest in the SX tank farm. Furthermore, information about the transport source term, particularly the timing of the leak, the volume of the leak, and the contents of the leaked fluid is not known with any certainty. Given the imperfect knowledge of input parameters and the key physical and chemical processes, the model can at best be used only qualitatively.

3.2.1 Soil Hydraulic Properties

The geologic description of the lithology suggest that five sediments types generally exist around tank SX-109. As shown above, these include backfill, Hanford fine sand, Early Palouse, Upper Ringold, and Middle Ringold formations. The general hydraulic properties of these sediments have been documented by Connelly et al. (1992). Hydraulic properties were summarized in the form of saturated water content, residual water content, and the fitted van Genuchten parameters α and n for each major sediment type. In

this study, we were interested in analyzing the effect of different layer sequences that could lead to capillary breaks. Modeling of water flow and contaminant transport under such conditions required the adoption of a water retention function that allowed for the definition of a distinct air entry value. Thus, the soil water retention curves were defined using the Brooks and Corey (1966) function and the Burdine (1953) relative permeability model. The Brooks-Corey function is defined as

$$\theta(\psi) = (\theta_s - \theta_r)\left(\frac{\psi_a}{\psi}\right)^{\lambda} + \theta_r; \qquad \psi \le \psi_a \tag{1}$$

where θ = volumetric water content
θ_s = saturated volumetric water content
θ_r = residual volumetric water content
ψ = soil water potential
ψ_a = air entry potential
λ = empirical coefficient related to the pore size distribution

Equation (1) was fitted to water retention data reported by Connelly et al. (1992). In the absence of a neutron probe calibration relationship, relative neutron counts were used as a basis in selecting the layer sequences. The soils chosen to demonstrate the effects of layering on water flow and transport and the fitted Brooks-Corey parameters are shown in Table 3. The lateral saturated hydraulic conductivity, K_x, was assumed to be 1.5 times the vertical saturated conductivity, K_z.

3.2.2 Transport and Contaminant-Porous Medium Interaction Parameters

In the vadose zone, it is known that very wide ranges of dispersivity exist (Beven et al. 1993). Furthermore, the common assumption that the dispersivity is equal to 0.1 of the travel distance, a concept borrowed from the groundwater field and commonly used at Hanford, cannot be justified. Unfortunately, there are no texture-dependent transport properties for the soils underlying these SX tank farm. Thus,

Table 3. Brooks-Corey Parameters for Selected Soils Identified Around Tank SX-109

Soil Type	θ_s ($m^3\ m^{-3}$)	θ_r ($m^3\ m^{-3}$)	ψ_a (cm)	K_s^x (cm s^{-1})	K_s^z (cm s^{-1})	λ
Backfill	0.2585	0	-9.206	1.239×10^{-3}	1.239×10^{-3}	1.838
Silty Sand	0.4272	0.086	-8.507	1.193×10^{-3}	7.700×10^{-4}	0.644
Gravel	0.194	0	-6.769	2.478×10^{-3}	1.239×10^{-3}	0.382
Pebbly Sand	0.5083	0.004	-0.484	1.650×10^{-1}	5.500×10^{-2}	0.239
Early Palouse	0.5094	0	-91.39	2.800×10^{-4}	1.400×10^{-4}	1
Upper Ringold	0.4183	0.034	-8.275	3.600×10^{-4}	1.800×10^{-4}	0.953
Middle Ringold	0.4215	0.034	-7.056	3.760×10^{-3}	1.880×10^{-3}	0.952

values of longitudinal (λ_L) and transverse (λ_T) dispersivity were estimated for the different stratigraphic units. In this study, no attempts were made to incorporate scale- or texture-dependent dispersivity. A conservative value of 1.0 m was assumed for the longitudinal dispersivity, λ_L, while a value of 0.1 m was assumed for the transverse dispersivity, λ_T.

In the absence of data describing the relationship between the K_d of ^{137}Cs and the concentration of competing ions, a range of values was chosen. Values of 0, 0.5, 3, and 37 mL g^{-1} were selected for ^{137}Cs and were applied at arbitrarily selected times for similarly selected durations. For the mobile species of interest, ^{99}Tc and NO_3^-, K_d was set to 0 mL g^{-1}. The half-lives of ^{137}Cs and ^{99}Tc were set to 30.17 yr and 2.13×10^5 yr, respectively. For all lithologic units, the effective molecular diffusion coefficient was set to 1×10^{-5} m^2 d^{-1}.

Estimates of the specific gravity of the supernatant range from 1.1 to 1.65 (Anderson 1990). Simulations were conducted with values of 1.0, 1.4, and 1.65. There were no data on viscosity. However, viscosity was calculated as a function of salt concentration based on a relationship developed for saltwater brines. The coupled flow and transport capabilities of STOMP were developed specifically for salt-water brines in which the maximum solute concentration is 0.2605 kg solute/kg solution or 312.6 kg solute m^{-3}. Simulation of salt (NO_3^-) transport from tank SX-109 with a specific gravity exceeding 1.4 required modification of the algorithms for computing brine properties (specific gravity and viscosity).

3.2.3 Initial Conditions

The initial conditions for water flow were defined as pressure head. In order to reduce the computational effort, a generalized analytical solution to the one-dimensional Richards' equation for infiltration in heterogeneous media (Rockhold et al. 1996) was used to generate the initial conditions. This solution required less than 10 seconds to run on a personal computer and reduced the number of time steps required by STOMP from over 300, when a hydrostatic equilibrium was used as the initial condition, to around 25 when the initial condition was generated by the analytical, steady-state method. For solution of the transport equations, initial concentrations of salt (NO_3^-), ^{137}Cs, and ^{99}Tc were all set to zero. The decay constants for ^{137}Cs and ^{99}Tc were specified to permit decay but the equations for their progeny were not solved.

3.2.4 Boundary Conditions and Sources

For the water flow equation, boundary conditions at the surface were specified as Neuman with the flux equal to the recharge rates of 0.5, 10, and 100 mm yr^{-1}. A variable recharge rate of 10 mm yr^{-1} for the first 20 years followed by 40% of annual precipitation was also used. On the surface, a zero flux boundary was established for ^{99}Tc, NO_3^-, and ^{137}Cs. The east and west boundaries were set to initial condition boundaries for flow and transport. The initial condition boundary is identical to in application to the Dirichlet boundary condition, with the exception that the primary variable is fixed to the initial value at the adjacent node (White and Oostrom 1996). The bottom boundary was located 16 m (52.5 ft.) below the water table and was specified as a Dirichlet boundary with a pressure equal to the hydraulic head. For solution of the transport equations, this boundary was specified as an outflow boundary. The outflow, or free exit boundary, permits the transport of solutes across the boundary by advection only.

The source function is poorly defined since very little is known about the historical leakage rate for the tank. Furthermore, there have been no studies aimed at recovering the effective source functions from the contaminant plume. In a recent progress report, Agnew (1996) reported that tank SX-109 showed the first unaccounted volume loss in December 1958, with continued long-term unaccounted losses. Hanlon (1996) reported 1965 as the date of first volume loss, while Anderson (1990) reported it as December 1957. Several estimates of leak volume have also been made. Estimated leak volumes range from 45 m^3 (Anderson 1990) to over 946 m^3 (GJPO 1996), and more recently 276 m^3 (Agnew 1996). In this study, it was assumed that a leak of 499.7 m^3 (132,000 gal) occurred in three stages (Figure 6).

In the first stage, a leak of 75.7 m^3 (20,000 gal) occurred over a 0.5 yr period starting in July 1964. In the second stage, a leak of 333.12 m^3 (88,000 gal) occurred over an 11-yr period, immediately after the first stage and finishing in 1973 when the tank was pumped to a minimum level. The leak is assumed to have started again in 1983, with a total of 90.85 m^3 (24,000 gal) lost through 1994 in an exponential fashion. There is no evidence to support the actual location of the leak, but in this study, the leak was assumed to have occurred over a 12-m section of the tank (Figure 5). Thus, in the first stage, the fluid leaked out at a rate of 4.79×10^{-6} m^3 s^{-1}. In the second stage, the rate was 1.319×10^{-6} m^3 s^{-1}, while the rate was variable in the third stage. Waste inventories for tank SX-109 suggest a concentration of 0.24 Ci L^{-1} for ^{137}Cs. This is equivalent to a total load of 1.199×10^{17} pCi contained in the simulated leak. The concentration of ^{99}Tc was 2.9×10^{-5} Ci L^{-1}, or 1.149×10^{13} pCi in the leaked fluid. The specific gravity of the

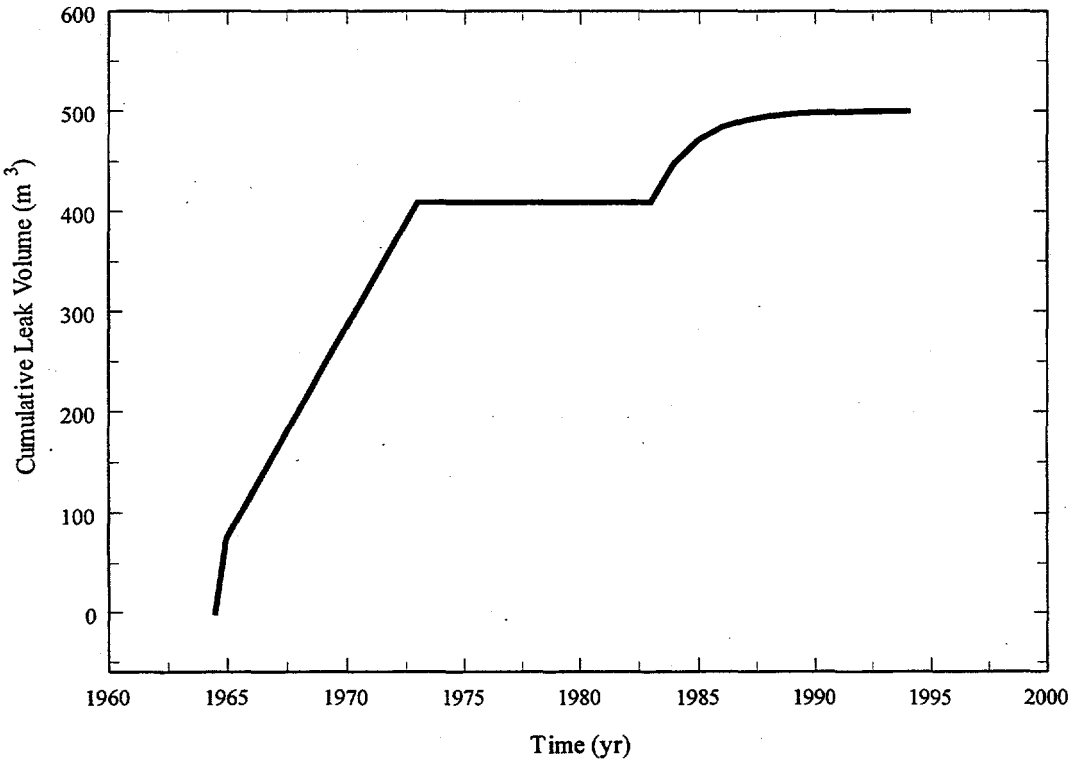

Figure 6. Hypothetical Release History Used in SX-109 Tank Leak Simulation. The Leak is Assumed to have Occurred in Three Stages, Finally Ending in 1994.

leaked fluid varied between 1.0 (no salt) to 1.65 (salt mass fraction of 0.25 g salt per g of solution). The loading rate for the salt was calculated as 9.45×10^4 kg s^{-1} in the first stage and 2.6×10^4 kg s^{-1} in the second stage.

3.2.5 Recharge

For the SX tank farm, no direct measure of net recharge is available. Therefore, it was necessary to estimate recharge. Three different approaches were used to determine recharge for the simulations. Estimates of recharge from meteoric sources (rainfall and snowmelt) that drains from the soil surface annually at the SX Tank farm are based on analyses for the Hanford Site as reported by Gee et al. (1992), Fayer and Walters (1995), and Fayer et al. (1996). Observations of water infiltration at similar sites and from lysimeter facilities indicate that as much as 100 mm yr^{-1} can infiltrate a coarse, gravel surface that is free of vegetation. For this reason, a value of 100 mm yr^{-1} was selected as a conservative estimate of maximum net recharge for simulating the tank SX-109 leak.

It should be noted that by fixing net recharge at 100 mm yr^{-1}, it is assumed that more than 60% of annual precipitation drains to the water table. The simulation of such a high rate of recharge is considered conservative for several reasons. First, the recharge rate of 100 mm yr^{-1} has been documented for very clean gravel surfaces but has not been confirmed for tank farm gravels. Drainage from bare sands has been shown to be on the order of about 70 mm yr^{-1} for the Hanford Site. Second, the simulation does not account for thermal effects, which could cause drying and possibly even lower recharge rates. Heat generated in the tank could produce steam and subsequently cause drying around the tanks, especially during the initial tank filling and for a some time thereafter (through the early 1970s). High temperatures could also promote wetting front instability due to the influence on viscosity. If the thermal regime around the tank were better known these effects could be more thoroughly analyzed.

To evaluate the effect of high heat load on net infiltration, a case was simulated with a recharge of 10 mm yr^{-1} for the duration of the simulation. The effect of variable recharge was also studied by setting recharge to 10 mm yr^{-1} for the period 1964 to 1983, followed by a recharge equal to 40% of the annual precipitation. Precipitation beyond 1996 was predicted using the WGEN model (Richardson 1981). A series of cases was also simulated in which the recharge was limited to 0.5 mm yr^{-1} and 10 mm yr^{-1} for the entire simulation. Table 4 summarizes the recharge rates used in the simulations. All simulations were run

Table 4. Summary of Recharge Rates in the Simulation of the Leak From Tank SX-109.

Simulation	Recharge Rate (mm yr^{-1})		
	1964-1973	1973-1983	1983-2015
Hanford Barrier	0.5	0.5	0.5
Low Rate	10.0	10.0	10.0
Variable rate	10.0	40 % precipitation	40% precipitation
High Rate	100.0	100.0	100.0

for 50 yr, following a 1000-yr simulation of infiltration to approximate steady-state moisture conditions around the tank before the leak. Table 5 summarizes some of the hypothetical cases simulated in this study.

An alternate conceptual model has been used to estimate migration rates of contaminants in tank farms at the Hanford Site as part of the Tank Waste Remediation Strategy Environmental Impact Statement (TWRS-EIS) (USDOE 1996). The TWRS-EIS describes the transport of contaminants by assuming the following conditions:

1) one-dimensional flow
2) steady-state conditions
3) constant recharge rates
4) idealized geometry based on simplified horizontal layering
5) low longitudinal dispersivities dependent on layer properties and thickness
6) simplified geochemistry based on constant a K_d.

The TWRS-EIS conceptual model will be used as a basis for comparing some of the current results.

Table 5. Summary of Transport Cases Simulated Using STOMP. All simulations assumed a leak volume of 500 m^3 (132,000 gal).

Case	Recharge Rate (mm yr^{-1})	Specific gravity	Stratification	K_d - ^{137}Cs (mL g^{-1})
1	variable	1.0	Simple	0.0
2	variable	1.4	Simple	0.0
3	variable	1.4	complex	0.0
4	0.5	1.4	complex	0.0
5	0.5	1.4	complex	37.0
6	10	1.4	complex	0.0
7	100	1.4	complex	0.0
8	variable	1.4	complex	3.0
9	variable	1.4	complex	37.0
10[a]	variable	1.4	complex	0.0/3.0
11[b]	variable	1.4	complex	0.0/37.0
12[c]	variable	1.4	complex	0.0/0.5/3.0/37.0
13[d]	variable	1.0	complex	0.0
14[e]	variable	1.4	complex	0.0

[a] K_d = 0 mL g^{-1} from 1965 through 1972 and 3.0 mL g^{-1} thereafter.
[b] K_d = 0 mL g^{-1} from 1965 through 1972 and 37.0 mL g^{-1} thereafter.
[c] K_d = 0 mL g^{-1} from 1965 for 0.5 yr, 0.5 through 1967, 3.0 through 1973, 37.0 through 1983, 3.0 through 1988, and 37 thereafter.
[d] Leak of 15 m^3 over a 15-yr period starting in July 1964. In all other cases, a leak of 500 m^3 was assumed.

4.0 Results and Discussion

The transport of contaminant beneath tank SX-109 was simulated in a series of hypothetical cases to investigate the effects of recharge rate, contaminant distribution coefficients, stratigraphy, and specific gravity of the leaked fluid on contaminant migration. The 14 cases shown in Table 5 are a subset of the total number of cases simulated and were chosen to show examples and trends. Discussions and conclusions are not necessarily inclusive but extend over the spectrum of results.

4.1 Distribution of Water Content and Water Flux

As a first step, a baseline case (Case 1) was simulated under the assumption that physical properties of the leaking REDOX waste were no different than those of pure water. This meant that there was no salt and the specific gravity was equal to 1.0, but the radionuclides ^{137}Cs and ^{99}Tc were assumed to be present. Characterization studies of tank wastes show that the specific gravity may vary between 1.2 and 1.65 (Anderson 1990). Thus, the impact of specific gravity of infiltration and waste migration was investigated in Case 2. Figure 7 compares the effect of specific gravity on the spatial distribution of moisture, at the end of the second stage of the leak in 1973, assuming a simplified stratigraphy.

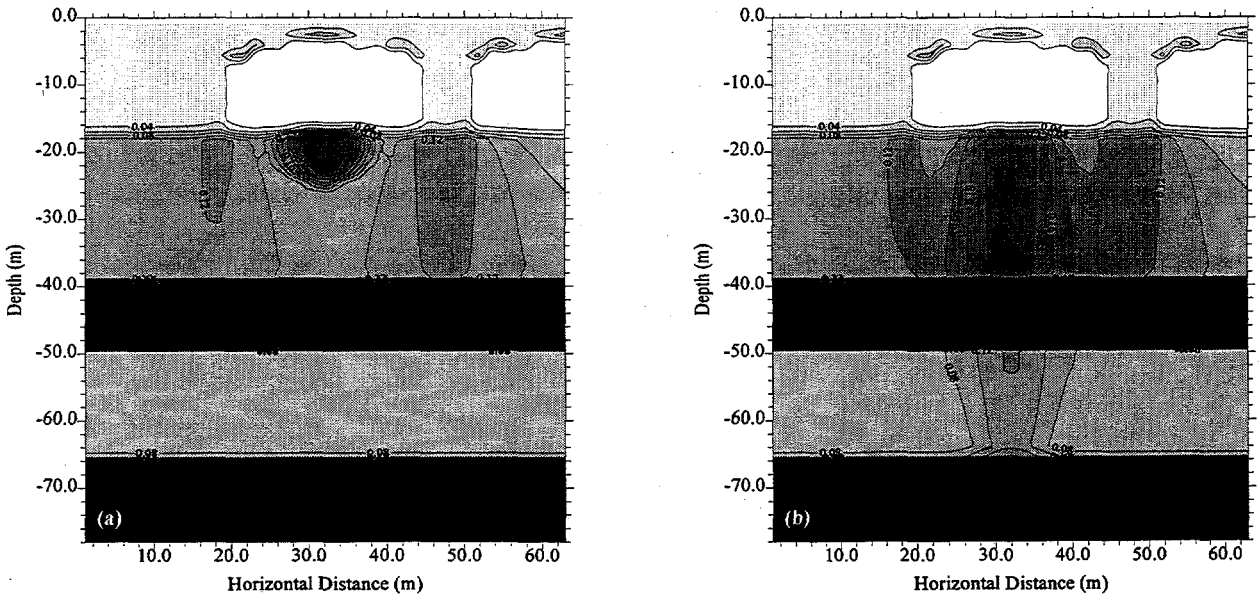

Figure 7. Simulated Volumetric Water Content ($m^3\ m^{-3}$) in 1973 Showing the Impact of Specific Gravity of the Leaked Fluid on Moisture Distribution in a Profile with Simplified Stratigraphy (a) Case 1, Specific Gravity = 1.0; (b) Case 2, Specific Gravity = 1.4.

In Figure 7a, the wet bulb is relatively symmetric suggesting that even after a leak of 409 m^3 (108,000 gal) of fluid, the relative magnitudes of gravitational and capillary forces were somewhat similar. The wet bulb was contained within an 11-m (36-ft.) depth below the tank, with a water content of around 0.12 $m^3\ m^{-3}$ at the wetting front. In contrast, the denser fluid produced a rather asymmetric wet bulb that reached the water table over the same period of time. Apart from the 40% increase in specific gravity, all other conditions remained unchanged in the simulation. Thus, the observed increase in asymmetry can only be explained by the relative contributions of gravity and capillarity on the flow field and is indicative of preferential flow.

Two main types of phenomena have been identified as contributing to preferential flow. The first is related to the instability of wetting fronts under certain conditions. The second is related to flow in continuous, non-capillary-sized pores and fractures. In this case, the asymmetry is due to an unfavorable density ratio that results when a dense fluid (brine) displaces a less dense fluid (water). The unfavorable ratio caused instability in the local wetting front, which resulted in the wetting front penetrating to greater depths in a relatively narrow zone.

These results provide the first indication as to why previous modeling attempts have all predicted arrival times in excess of 10^3 yr for mobile contaminants, even at high recharge rates. None of the previous attempts at modeling tank leaks and contaminant migration at the Hanford Site considered the impact that infiltration of dense fluids into an unsaturated soil can have on the resulting water fluxes and distribution of moisture within the soil. Not only did these models not consider the specific gravity of the leaking fluid, they never considered the impact of small-scale textural changes on the physics of flow in the vadose zone.

The impact of small-scale textural variations on the distribution of moisture is illustrated in Figure 8, which compares Case 2 and 3. Figure 8a (Case 2) shows the water content distribution under a simplified stratigraphy. In Case 3, soil lenses identified in Figure 3 were included, as were the sloped interfaces. The increase in water content at the interface between the fine and coarse textured soils, as well as the lower water content in the coarse textured layers, shows the impact of textural discontinuities on water flow (Figure 8b). The occurrence of fine-textured lenses over coarser layers resulted in a capillary break, which would normally impede infiltration. Under saturated conditions, the coarse layers would then act as zones of high velocities for contaminant migration and would result in significant lateral migration of contaminants. Under such conditions, it would be difficult to determine the source of contaminants observed at a borehole sandwiched by two or more tanks. Ignoring small-scale variations in texture results in an overestimation of the penetration depth of leak fluids, even when the specific gravity of the infiltrating fluid is ignored, and would have a similar impact on the predicted movement of dissolved contaminants.

The effect of recharge rate on moisture distribution is illustrated with the results of Cases 3, 4, 5, and 6 in 1983 (Figure 9). Under a recharge of 0.5 mm yr^{-1}, the rate of advance of the wetting front was significantly reduced, despite using the same leak rate (Figure 9a). The slower rate of advance of the wetting front is due to the lower antecedent water content. Soil at a lower initial water content would require more of the infiltrating tank fluid to fill the pore space in order to reach the steady-state water content characteristic of the leak rate. Thus, even under the high specific gravity, the leaked fluid would not have penetrated very deep into the profile. The reduced rate of advance of the wetting front would have also

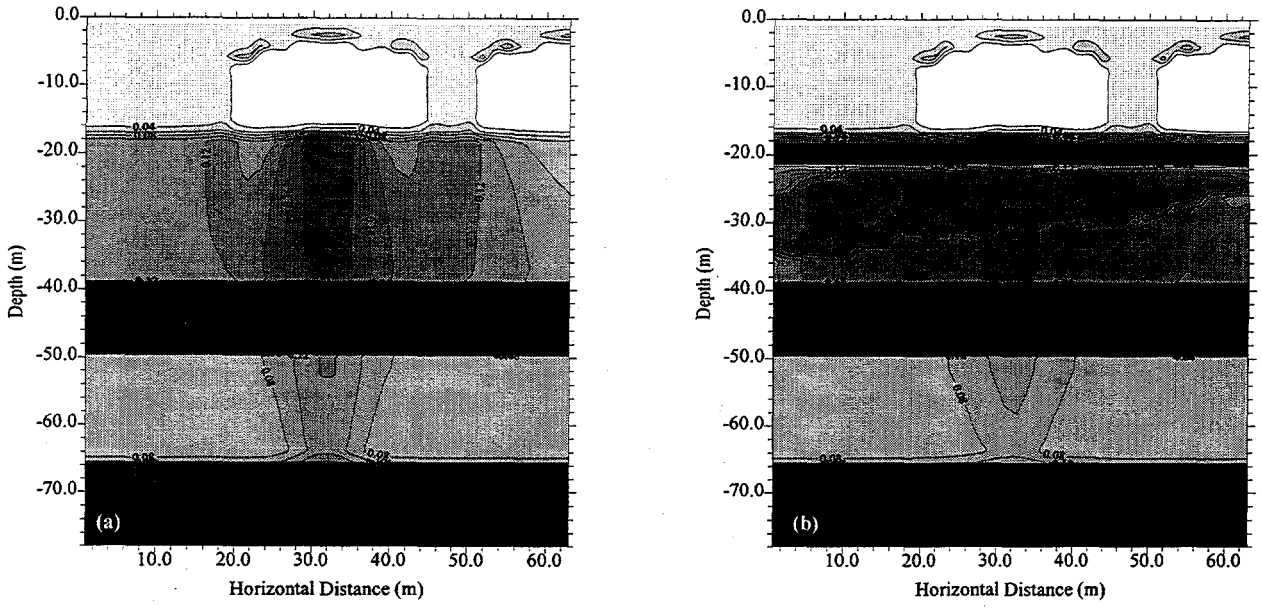

Figure 8. Simulated Volumetric Water Content ($m^3\ m^{-3}$) in 1973 Showing the Impact of Stratigraphic Detail on Moisture Distribution in a Profile with Simplified Stratigraphy (a) Case 2, Simple Stratigraphy, and (b) Case 3, Complex Stratigraphy, Including Lenses <0.6 m Thick.

reduced the rate of migration of contaminants. An increase in recharge rate to 10 mm yr^{-1} resulted in a significant increase in the lateral and vertical spread of moisture (Figure 9b). At this recharge rate, the soil water potential moved closer to the air entry pressure of the coarse layers and breakthrough started, as can be seen, between 30 and 38 m (98 and 125 ft.) directly below the tank in Figure 9b. A similar trend is observed at the variable recharge rate (Figure 9c) and at 100 mm yr^{-1} (Figure 9d).

Regardless of the specific gravity, the level of stratigraphic detail, or recharge rate, one persistent feature is observed in the effect of infiltrating meteoric water on the moisture conditions over the tank domes and around the periphery. When compared to the surrounding soil, water content was generally higher directly above the tank domes and around the tank perimeter. Above the tank domes, water content was as much as three times higher than in the surrounding backfill material (0.03 $m^3\ m^{-3}$). Around the perimeters, water content reached as high as 0.25 $m^3\ m^{-3}$, compared to the surrounding backfill material (0.18 $m^3\ m^{-3}$). The increase in water content around tank perimeters can be attributed to the enhanced recharge, also known as the "umbrella effect", caused by the shedding of water from the impermeable tank domes. Figure 10 compares the recharge at the depth of the tank base (16 m [52 ft.]), at nodes 6 (x = 11 m [36 ft.], see Figure 5) and node 26 (x = 47 m [154 ft.], see Figure 5) in Case 3.

Recharge at the surface was fixed at 10 mm yr^{-1} until 1973, after which it increased to 40% of the natural precipitation. At x = 11 m, recharge is not influenced by tank shedding, while at x = 47 m, both tanks SX-109 and SX-108 contribute to the recharge. Under the fixed recharge, the water flux between the two tanks was more than twice the recharge rate. Under the variable rate, the recharge between the two tanks ranged between 1.8 and 4.6 times that observed away from the tank, depending on precipitation.

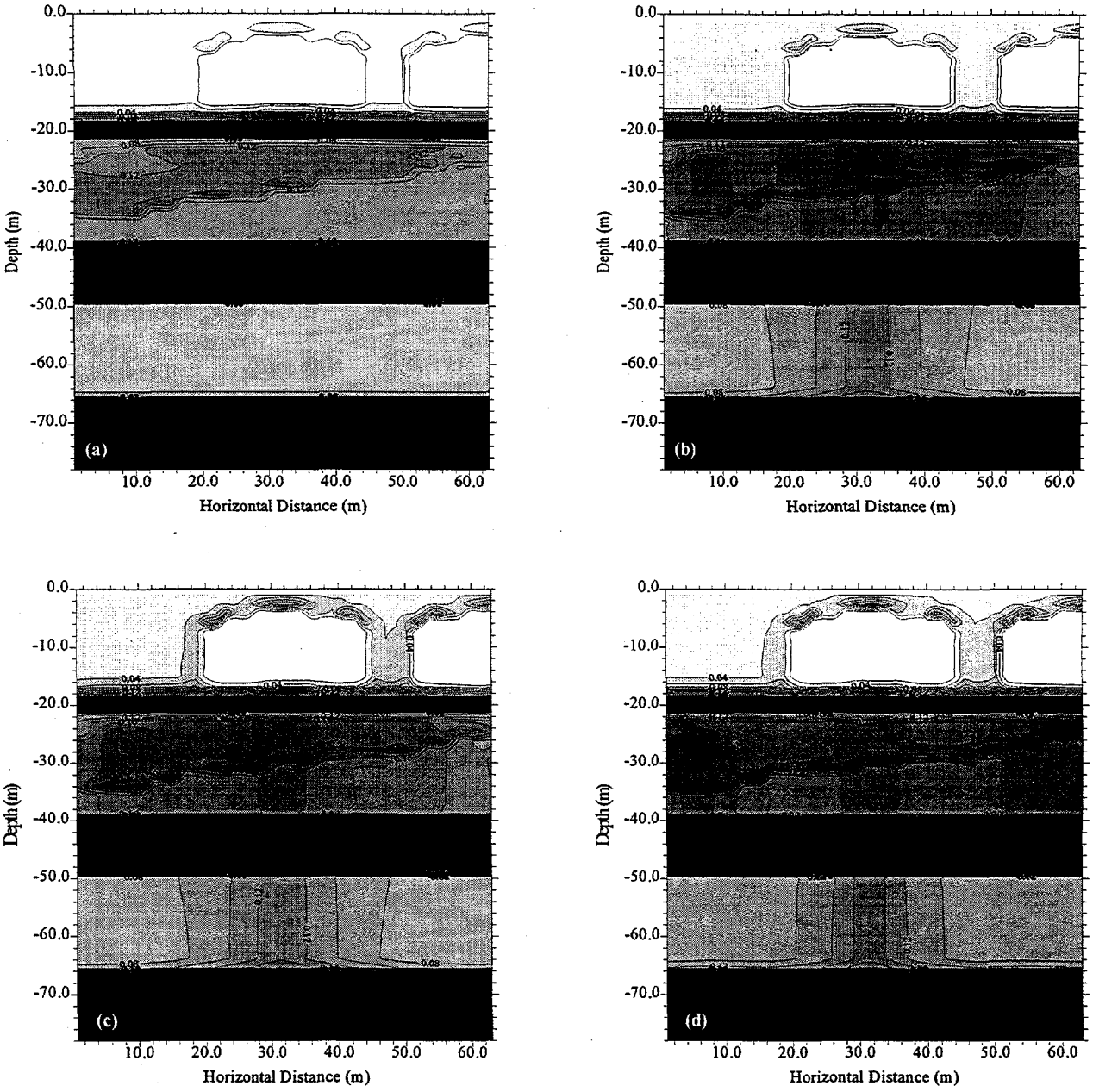

Figure 9. Simulated Volumetric Water Content ($m^3\ m^{-3}$) in 1973 Showing the Impact of Recharge Rate, J_w, on Moisture Distribution in a Profile with Complex Stratigraphy (a) Case 4, 0.5 mm yr^{-1}, (b) Case 6, 10 mm yr-1, (c) Case 3, J_w Variable, and (d) 100 mm yr^{-1}.

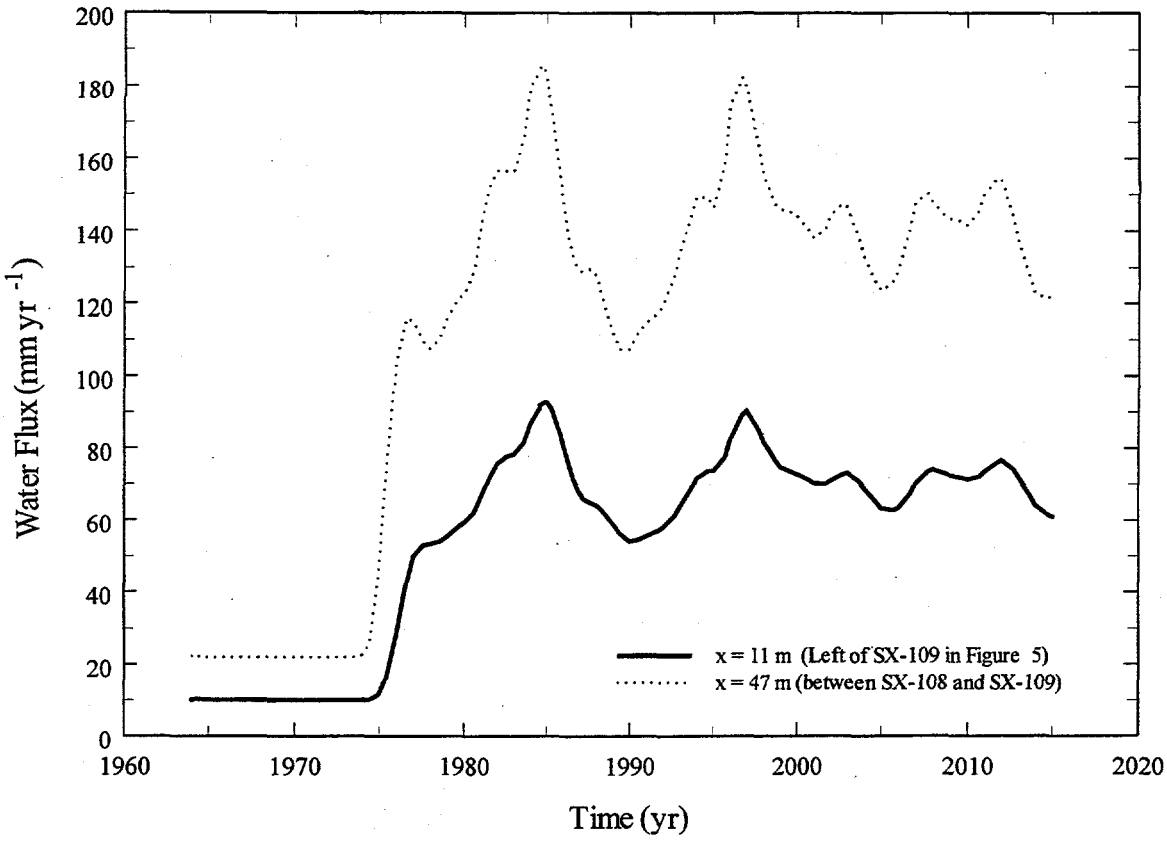

Figure 10. Comparison of Water Flux Between Two Tanks and Away From a Tank at a Depth of 16 m, Showing the Umbrella Effect (Case 3). Recharge Between the Tanks Ranged From 1.8 to 4.6 Times Higher Than the Imposed Recharge Rate.

This could have a serious impact on contaminant migration between tanks. The boreholes used for monitoring are located within the general zone of enhanced recharge and could very well serve as short circuits for any contaminants that might have reached the casings. Because the "umbrella effect" cannot be incorporated into one-dimensional models, the TWRS-EIS would have overestimated travel time to the water table.

Since the contaminants of interest, NO_3^-, ^{99}Tc, and ^{137}Cs, were dissolved in the tank fluids, movement of water would result in the movement of these contaminants, depending on the degree of solute-soil interaction. In the following sections, the migration of ^{137}Cs and ^{99}Tc are analyzed.

4.2 Transport of ^{137}Cs

Cesium-137 is potentially very hazardous because of its high specific activity. Many of the studies aimed at quantifying the sorption of ^{137}Cs were conducted in agricultural soils and suggest that ^{137}Cs is

strongly adsorbed onto clay and organic matter particles in a nonexchangeable fashion. Adsorption onto soils and sediments is rapid with distribution in undisturbed soils showing an exponential decrease with soil depth (Beck 1966, Ritchie et al. 1972). A number of recent studies have shown that in abnormal chemical environments (highly saline solutions), the K_d of ^{137}Cs decreases with increasing concentration of Na^+ and can be very close to 0 mL g^{-1}. Serne and Burke (1997) were unable to reproduce the high temperatures and exact chemical profile characteristic of REDOX waste. However, they reported K_ds from 20 to 37 mL g^{-1} for ^{137}Cs in a simulated waste at room temperature and cited K_ds less than 1.0 mL g^{-1} from studies of other high-level waste with lower pH and aluminum concentrations than REDOX wastes. These results suggest that ^{137}Cs has the potential to move fairly rapidly during the early years following a leak, a hypothesis that is supported by field observations. In the following sections, the results of ^{137}Cs transport simulations that would have resulted from a leak from tank SX-109 are summarized. All concentrations of ^{137}Cs are expressed in pCi g^{-1}.

As shown in section 4.1, the specific gravity of the tank fluid can have a significant impact on water flow and therefore contaminant transport. Figure 11 illustrates the impact of specific gravity on the migration of ^{137}Cs through the vadose zone beneath tank SX-109 assuming a simplified stratigraphy and no sorption.

Under a variable recharge and a leak of 409 m^3 (108,000 gal) ^{137}Cs had been transported to 62 m (203 ft.) by 1973 (Figure 11a). The hydraulic gradient alone was insufficient to move the fluid much beyond the Early Palouse soil, and significant lateral spreading occurred at the interface with the Hanford

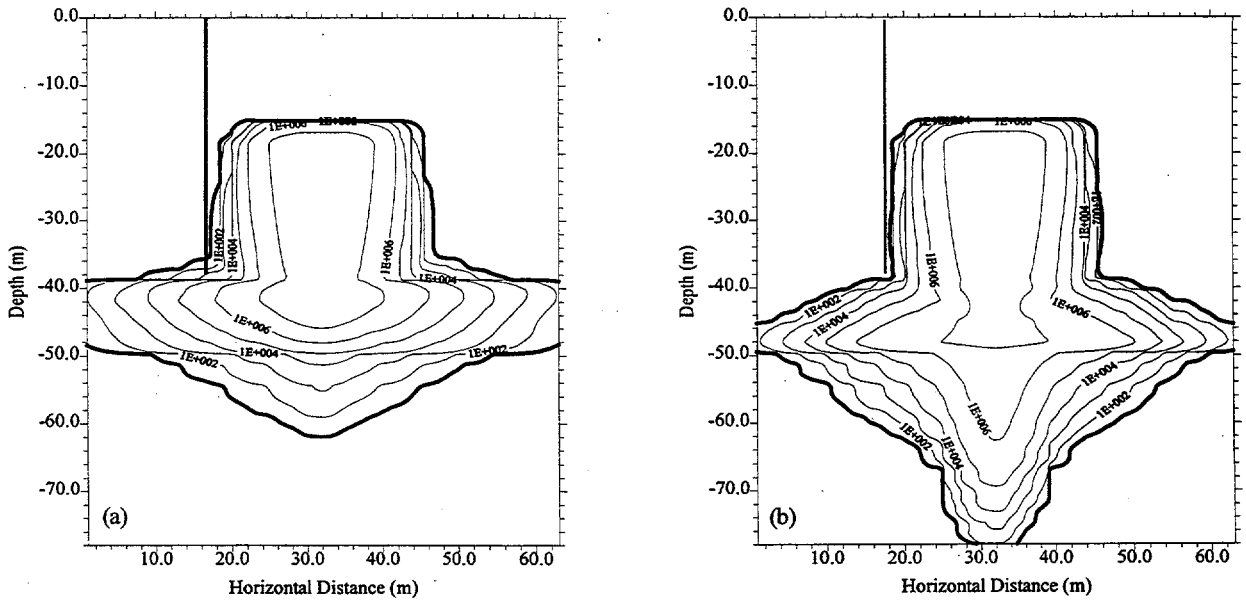

Figure 11. Simulated ^{137}Cs Concentration (pCi g^{-1}) in 1973 Showing the Impact of Specific Gravity on Plume Migration With a Simplified Stratigraphy Under a Variable Recharge and K_d= 0 mL g^{-1} (a) Case 1, Pure Water, and (b) Case 3, Specific Gravity =1.4. The Vertical Line at 17.6 m on the X-axis Represents the Borehole. The Bold Isopleth is 10 pCi g^{-1}.

fine sand. Under the same conditions but with a more realistic specific gravity (Case 2), there was less lateral spreading at the interface and the 10 pCi g^{-1} isopleth extended beyond the water table, even exceeding the 80-m (262-ft) depth (Figure 11b). Predictive modeling of ^{137}Cs migration must therefore account for the specific gravity of the tank fluid.

In earlier modeling studies, another simplifying step was assume that impact of small-scale textural changes in the vadose zone were negligible. Figure 12 illustrates the impact of small-scale textural variations on contaminant migration by comparing Cases 2 and 3. With a simplified stratigraphy, transport was primarily vertical in the first 25 m (82 ft.) below the tank (Figure 12a). The contaminant plume started to move laterally at the interface between the Hanford unit and the Early Palouse layer at the 40-m (131-ft.) depth, but was still able to penetrate the layer. The absence of the confining layer at 20 m (66 ft.) prevented the contaminant from spreading laterally. While the borehole showed no contamination at this depth, concentrations in excess of 10 pCi g^{-1} were present at the 38 m (125 m) depth (bottom of the borehole). By 1973, ^{137}Cs had also crossed the water table. These results are not in agreement with field observations as there is no evidence of widespread ^{137}Cs contamination in the soil profile down to the water table.

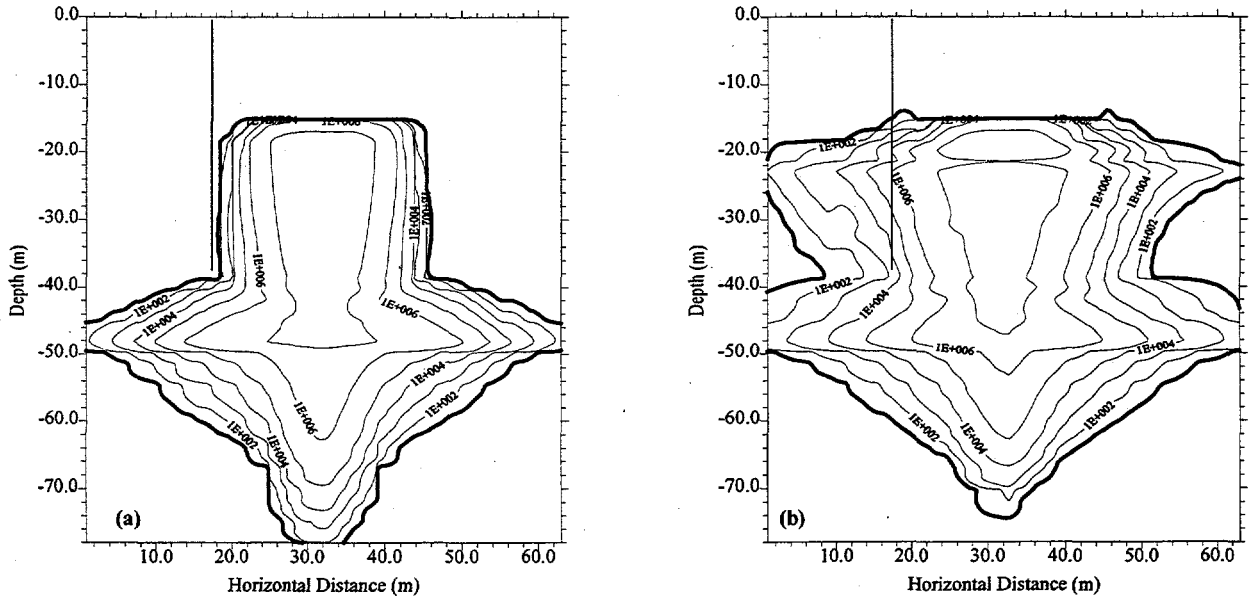

Figure 12. Simulated ^{137}Cs Concentration (pCi g^{-1}) in 1973 Showing the Impact of Stratigraphic Detail on Plume Migration Under a Variable Flux and $K_d = 0$ mL g^{-1}, (a) Case 2, Simple Stratigraphy, and (b) Case 3, Complex Stratigraphy. The Borehole is Shown at 17.6 m on the X-axis. The Bold Isopleth is 10 pCi g^{-1}.

In contrast, inclusion of the small-scale textural variations resulted in significant lateral spreading at the 20-m (66-m) depth (Figure 12b). The plume also moved preferentially along the sloped interface at the 32-m (105-ft.) depth. By 1973, a leak from tank SX-109 would have impacted monitoring wells between SX-109 and SX-108 making it impossible to accurately determine the source. The borehole adjacent to SX-109 showed high concentrations of ^{137}Cs down to its 38 m (125 ft.) maximum depth. However, these

results also show high concentrations of ^{137}Cs crossing the water table by 1973, an occurrence that is not supported by field observations. This suggests other mechanisms might be controlling the rate of migration. Recall that all of the cases thus far have made the conservative assumption of a K_d of 0 mg l^{-1} under a single recharge scenario.

Figure 13 shows the impact of the assumed recharge rate on the migration of ^{137}Cs. In the four cases (Cases 3, 4, 6, and 7), the K_d was fixed at 0 mL g^{-1} and a complex stratigraphy was assumed. By 1983, even after a leak of 409 m^3 (108,000 gal), ^{137}Cs moved in a predominantly lateral plane and did not migrate beyond a depth of 30 m (98 ft) or 15 m (49 ft.) below the tank, as shown in Figure 13a. A 20-fold increase in recharge to 10 mm yr^{-1} significantly increased the rate of migration, spreading ^{137}Cs throughout the entire simulation domain (Figure 13b). A variable recharge had a similar impact (Figure 13c). A recharge of 100 mm yr^{-1} resulted in transport that was predominantly vertical. This predominantly vertical migration occurred because at such a high recharge rate, the air entry potentials of the capillary breaks were easily violated resulting in less lateral spreading and early breakthrough at the water table. Based on over 10 years of data collected at Hanford, the variable recharge is probably the most realistic representation of the actual recharge. These results not only highlight the need for accurate estimates of recharge in the tank farms, but show that controlling recharge is a useful approach to limiting contaminant migration in the Hanford tank farms.

There is no evidence of ^{137}Cs in the groundwater beneath the SX Tank farm, since none has been observed in any downgradient wells. Therefore, it was necessary to investigate other variables that could influence ^{137}Cs migration in the vadose zone. Given the range of K_d values suggested for ^{137}Cs and the uncertainty about field values, the impact of K_d was evaluated by running simulations with constant K_ds of 0.0, 3.0, and 37 mL g^{-1} and various combinations (Table 5). All simulations assumed a leak volume of 500 m^3 (132,000 gal) and a variable recharge (Table 4). The 1996 results of these simulations are compared in Figure 14. Under a variable recharge, a K_d = 0 mL g^{-1} for the duration of the simulation is rather unrealistic (Figure 14a). Based on the data from borehole monitoring, there is no evidence of a widespread distribution of ^{137}Cs in the vadose zone of any of the tank farms. Increasing the K_d to 3 mL g^{-1} resulted in a more compact plume in which the 10 $pCig^{-1}$ isopleth was contained at the 40-m (131-ft.) depth. There was enough lateral spreading at the 20-m (66-ft.) depth for the migrating plume to intercept the borehole (Figure 14b). Boreholes between tanks SX-109 and SX-108 also would have been impacted, again highlighting the difficulty in identifying the exact source of a leak with vertical borehole monitoring alone.

While there is evidence of a dependence of K_d on the concentration of competing ions such as Na^+, there are no site-specific data that could be applied in this investigation. Nevertheless, data reported by Raymond and Shdo (1966) suggest that ^{137}Cs did indeed move quite rapidly within the first few years after a leak, suggesting an initially low K_d. In Case 11, a K_d = 0 mL g^{-1} was assumed for the first 8 yr, after which it was increased to 37 mL g^{-1}. The results for 1996 are shown in Figure 14c. Assuming a K_d of 0 mL g^{-1} for 8 yr resulted in ^{137}Cs spreading throughout the simulation domain and crossing the water table by 1996 Increasing the K_d to 37 mL g^{-1} essentially stopped any further migration, and the plume shrank somewhat due to radioactive decay. The borehole showed high concentrations of ^{137}Cs over its entire length, a result that is not supported by field observations. This result suggests that ^{137}Cs might have

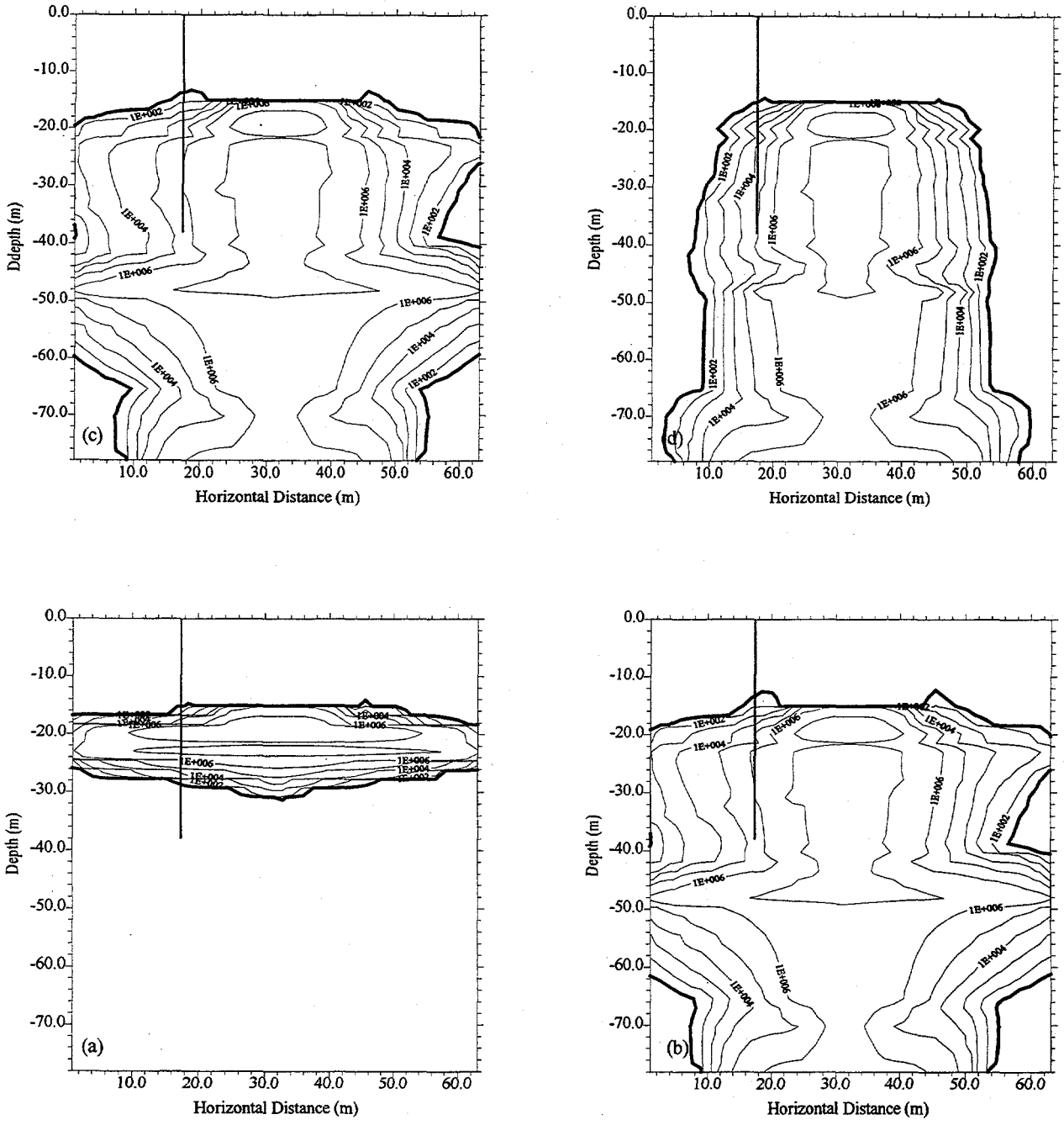

Figure 13. Simulated ^{137}Cs Concentration (pCi g^{-1}) in 1983 Showing the Impact of Recharge Rate, J_w, on Plume Migration With a $K_d = 0$ mL g^{-1}, (a) Case 4, $J_w = 0.5$ mm yr^{-1}, (b) Case 6, $J_w = 10$ mm yr^{-1}, (c) Case 3, Variable Recharge, and (d) Case 7, $J_w = 100$ mm yr^{-1}. The Borehole is Shown at 17.6 m on the X-axis. The Bold Isopleth is 10 pCi g^{-1}.

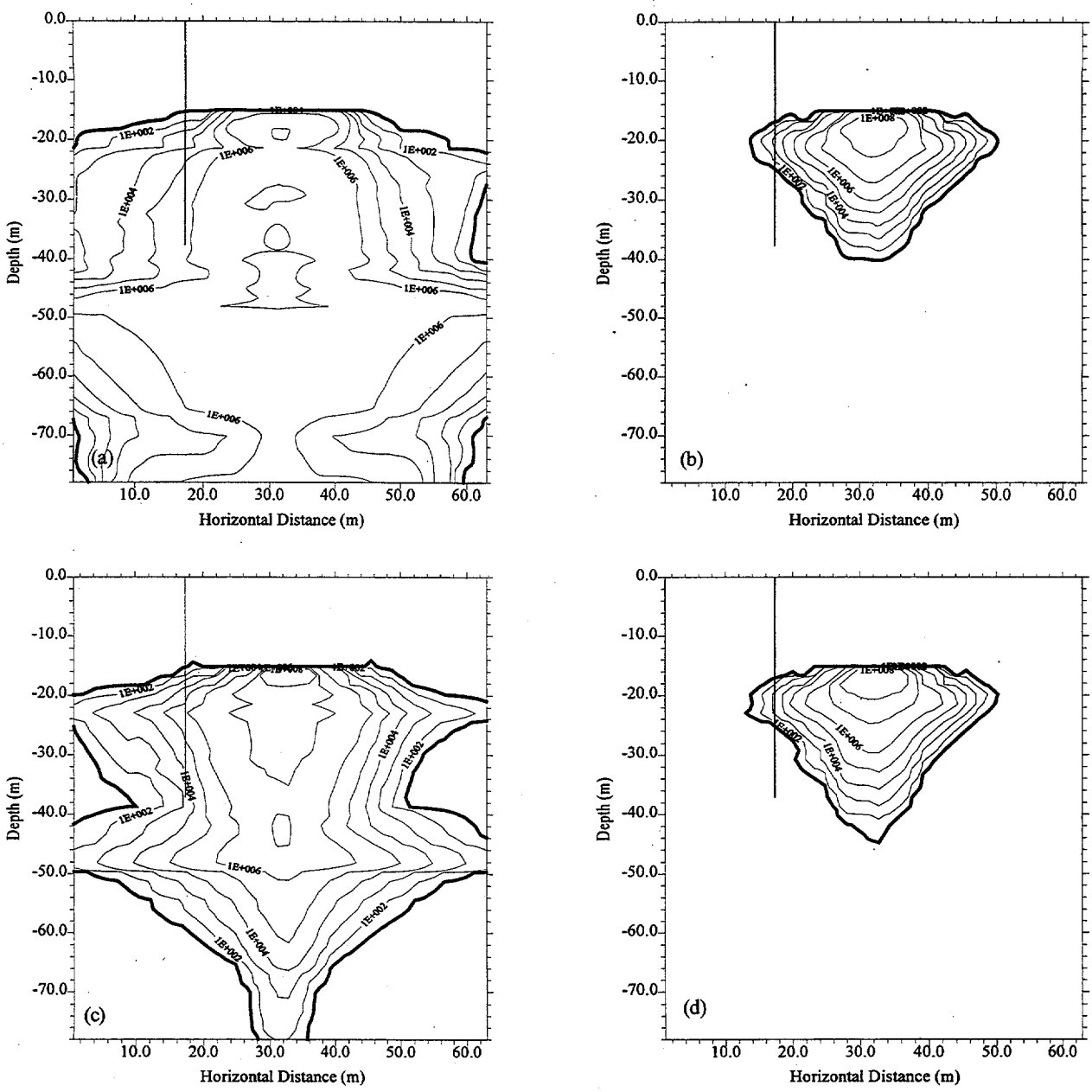

Figure 14. Simulated ^{137}Cs Concentration (pCi g^{-1}) in 1983 Showing the Impact of K_d, on Plume Migration Under a Variable Recharge Rate (a) Case 3, K_d = 0 mL g^{-1}, (a) Case 8, K_d = 3.0 mL g^{-1}, mm yr^{-1}, (b) Case 11, K_d = 0.5 and 3.0 mL g^{-1}, and (d) Case 12, K_d = 0/0.5/ 3.0/ 37/3.0/37.0 mL g^{-1} (see Table 5). The Borehole is shown at 17.6 m on the X-axis. The Bold isopleth is 10 pCi g^{-1}.

moved under a low K_d for a shorter period but one long enough for the plume to reach the 20-m (66-ft.) depth where most of the boreholes show high concentrations. Case 12 was run in an attempt to capture such a scenario(see Table 5). A $K_d = 0$ mL g^{-1} for the first 0.5 yr of the leak allowed ^{137}Cs to move to 20 m (66 ft.) and out to the borehole (Figure 14d). Progressively higher K_ds prevented migration beyond the 40-m (131-ft.) depth.

In the previous cases, a relatively large leak was assumed to have occurred over a short time. While tank leaks represent a very small amount of the total waste released, many leaks were not actually measured (Agnew 1996). Furthermore, only those leaks that actually resulted in measurable volume loss from a tank are included in leak estimates. To evaluate the impact of release history, it was assumed that tank SX-109 leaked a total of 15 m^3 (4000 gal) over a 15-year period, starting in July 1964. A leak of this size was chosen to allow a comparison with the modeling results of the TWRS-EIS (USDOE 1996). Case 13 was simulated with the assumption that the properties of the leaked fluid were identical to those of water, as assumed in the TWRS-EIS, while Case 14 assumed a specific gravity of 1.4. Figure 15 shows the results of these two cases in 1996, 17 years after the leak ceased.

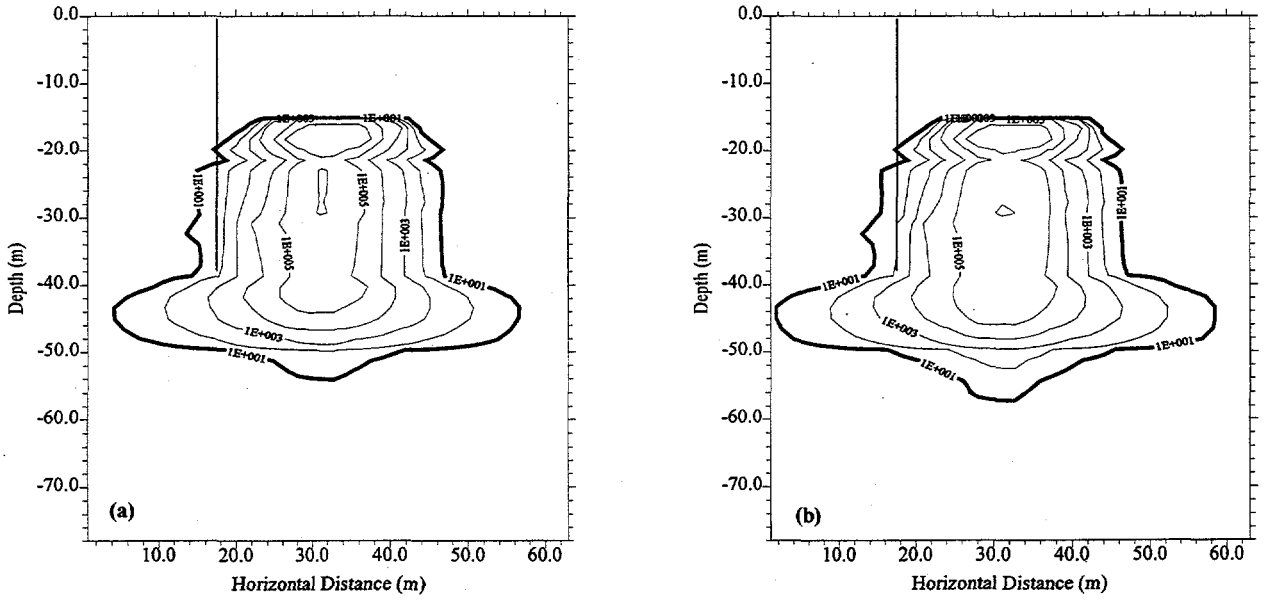

Figure 15. Simulated ^{137}Cs Concentration (pCi g^{-1}) in 1996 Showing the impact of a Change in Release history. A Total of 15 m^3 was Leaked over 15 yr (a) Case 12, Specific Gravity = 1.0, and (b) Case 13, Specific Gravity = 1.4. A Variable Recharge Rate and a $K_d = 0$ mL g^{-1} were Assumed. The Borehole is Shown at 17.6 m on the X-axis. The Bold isopleth is 10 pCi g^{-1}.

Unlike Case 3 (Figure 14c) in which a leak of 500 m^3 (1.3 x 10^5 gal) was assumed, the plume is more compact. Despite assuming a K_d of 0 mL g^{-1}, the 10 pCi g^{-1} isopleth did not exceed 54 m (177 ft.), remaining well above the water table (Figure 15a). Accounting for the specific gravity of the leaked fluid resulted in more spreading of the plume and a 4-m (13-ft.) increase in the depth of penetration (Figure 15b). In both cases, the borehole showed concentrations of around 100 pCi g^{-1} from 22 m (72 ft.) onward. These

results suggest that knowledge of the release history is just as important as the physics and chemistry of flow and transport in predicting the future migration of tank wastes.

In the preceding sections, the impact of several hydrologic and geochemical parameters on the migration of ^{137}Cs were qualitatively summarized. Vertical profiles of ^{137}Cs were extracted from the contour plots, at the location of the borehole, to permit quantitative analysis. Examples of these profiles comparing the effect of K_d under a variable recharge are shown in Figure 16. All of the profiles were analyzed by moment analysis in order to quantify the effects of the different variables. Moment analysis has been used to obtain velocities and dispersion parameters of packed beds in chemical engineering, with more recent applications to transport in unsaturated soils (Appendix A). Table 6 summarizes the first and second central moments of the vertical profiles comparing the effect of the different variables. The first central moment, M_1, is the mean depth of travel, or the location of the center of mass, while the second moment, M_2, represents the variance about the mean which is related to the amount of dispersion.

If the specific gravity of the leaked fluid and small-scale lithologic information are not taken into account, erroneous conclusions about the extent of waste migration can result. Increasing the specific gravity by 40 % increased the mean depth (M_1) of travel by 6 m (20 ft.) and tripled the variance (M_2). Including small-scale variation in stratigraphy decreased M_1 but almost doubled the variance. Controlling recharge limited M_1 to 21.57 m (71 ft.), only 5.6 m (18 ft.) below the tank, and also controlled large-scale spreading in the vertical but not lateral direction. While M_1 generally increased with recharge rate, there was no obvious trend in M_2. The degree of interaction between ^{137}Cs and the soil, as defined by K_d, had by far the greatest impact on migration of the plume. Profiles obtained under constant K_d values, both high and low, showed little agreement with field-measured profiles. In contrast, profiles obtained under variable K_ds profiles showed good agreement in both the mean depth of travel and the spread about the mean (M_2). Decreasing the leak volume by 97% and the pulse duration decreased M_1 by 7 m (23 ft.) and decreased M_2 by a factor of more than 6. Analysis of the ^{137}Cs distributions showed that, except under extreme recharge rates and very low K_ds, the contaminant was contained within a 40-m (131-ft.) depth.

To further demonstrate, in a qualitative sense, the similarity between the simulated results for the most likely scenario and field observations, a time series plot of the total mass of ^{137}Cs at the 20-m (66 ft.) depth was generated. Recall that Price (1996) showed an increasing count rate on borehole 49-09-09 at this depth. Simulated profiles from Case 12 for the years 1973 through 1998 were integrated over depth and the result (pCi g^{-1} m) plotted as a function of time (Figure 17).

The results show a gradual accumulation of mass over time, with a sharp increase occurring just after 1983. Recall that in the simulated release history, (Figure 6) tank SX-109 started to leak again in 1983. Therefore, the K_d was deceased from 37 mL g^{-1} to 3.0 mL g^{-1} from 1983 through 1988, after which it was increased again to 37 mL g^{-1}. The rate of accumulation of mass declined in 1986, most likely due to a decline in recharge. Unlike the field observations, these results show a decline in accumulated mass beyond 1988. This is the point at which the K_d was assumed to increase to 37 mL g^{-1}. The fact that our simulation does not show a continued increase is due to two factors: 1) our release history assumed that the leak stopped in 1994, and 2) it was assumed that the K_d increased from 3.0 to 37 mL g^{-1} in 1988. These assumptions are based on a crude analysis of data from a single borehole and on what is assumed about the current status of tank SX-109 and are therefore somewhat subjective. However, within the limits of the

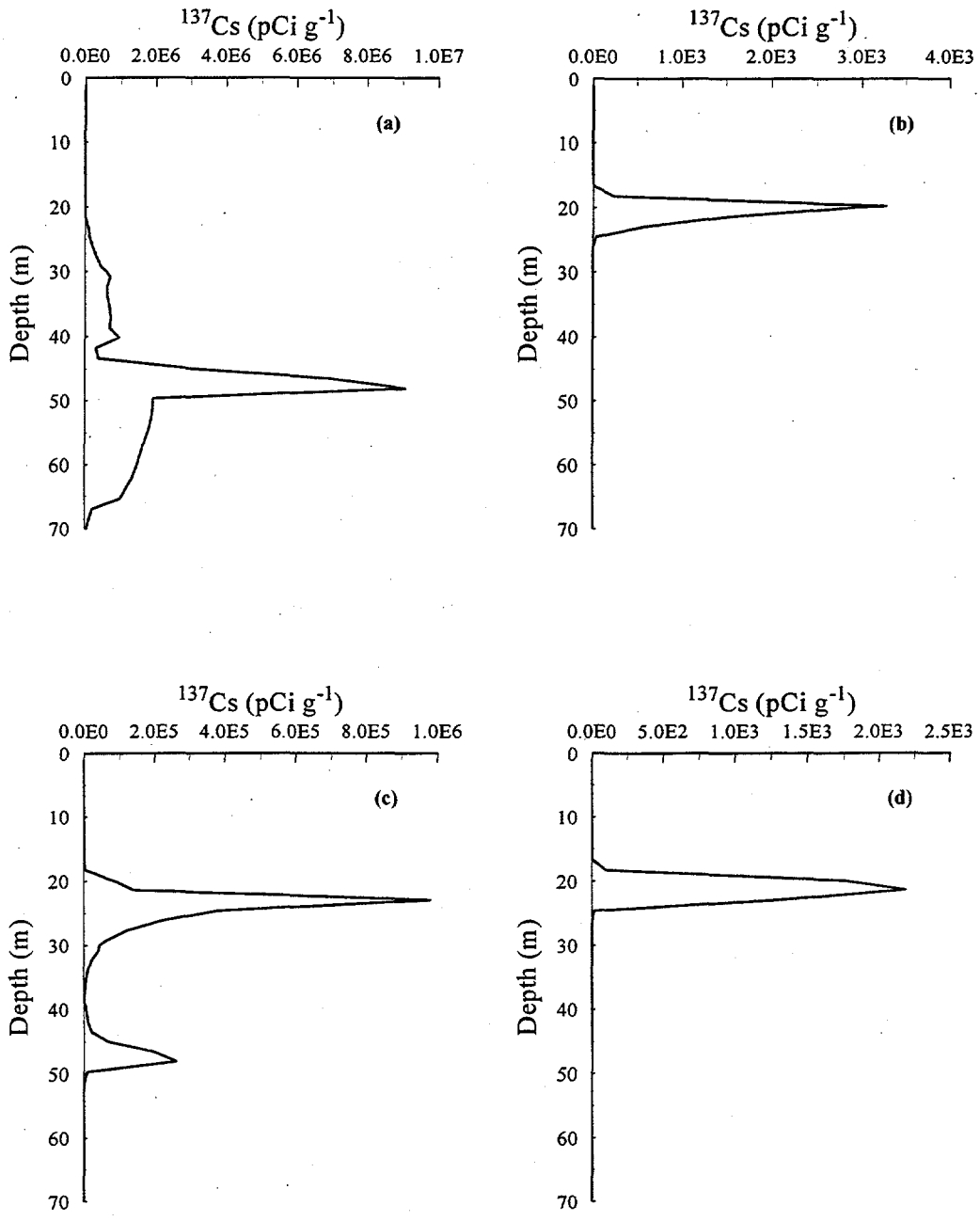

Figure 16. A Comparison of Simulated ^{137}Cs (pCi g^{-1}) Profiles at the Borehole in 1996 Showing the Impact of a K_d (a) Case 4, K_d = 0 mL g^{-1}, (b) Case 8, K_d = 3 mL g^{-1}, (c) Case 10, K_d = 0/3.0 mL g^{-1}, (d) Case 12, K_d = 0.0/0.5/3/37/3/37 mL g^{-1} (see Table 5).

Table 6. Moment Analysis of the Resident Probability Density Functions of ^{137}Cs

Comparison	Case	Description	M_1 (m)	M_2 (m^2)
Specific gravity	1	1.0	46.39	13.90
	2	1.4	52.22	40.32
Stratification	2	Simple	52.22	40.32
	3	Complex	49.10	73.21
Recharge	4	0.5 mm yr^{-1}	21.57	3.29
	6	10 mm yr^{-1}	47.05	99.39
	3	variable	49.10	73.21
	7	100 mm yr^{-1}	54.02	80.61
K_d	4	0.0 mL g^{-1}	49.10	73.21
	8	3.0 mL g^{-1}	20.57	1.90
	9	37.0 mL g^{-1}	19.63	1.09
	10	0/3.0	32.97	127.0
	11	0/37.0	29.19	94.30
	12	0.0/0.5/3.0/37.0	21.27	1.98
Release History	13	Volume = 15 m^3	42.44	11.42
	2	Volume = 500 m^3	49.10	73.21

analysis, these results are in relatively good agreement with the field observations (Figure 2) and lend support to the conceptual model. A thorough analysis of the changes in the rate of mass accumulation at the boreholes could provide more insight into the geochemical and transport processes. For example, the continued accumulation of ^{137}Cs at 41-09-09 suggests a source of ^{137}Cs with a very low K_d, such as would result from an active leak. These results also suggest that accurate estimates of recharge in tank farms and a proper description of the relationship between the K_d of ^{137}Cs and the concentration of competing ions in the infiltrating water are the two most important pieces of information necessary for success in predicting leak migration in the vadose zone. A thorough analysis of existing data coupled with miscible displacement experiments in the laboratory would provide the necessary relationships for incorporation into a numerical model (Saiers and Hornberger 1996).

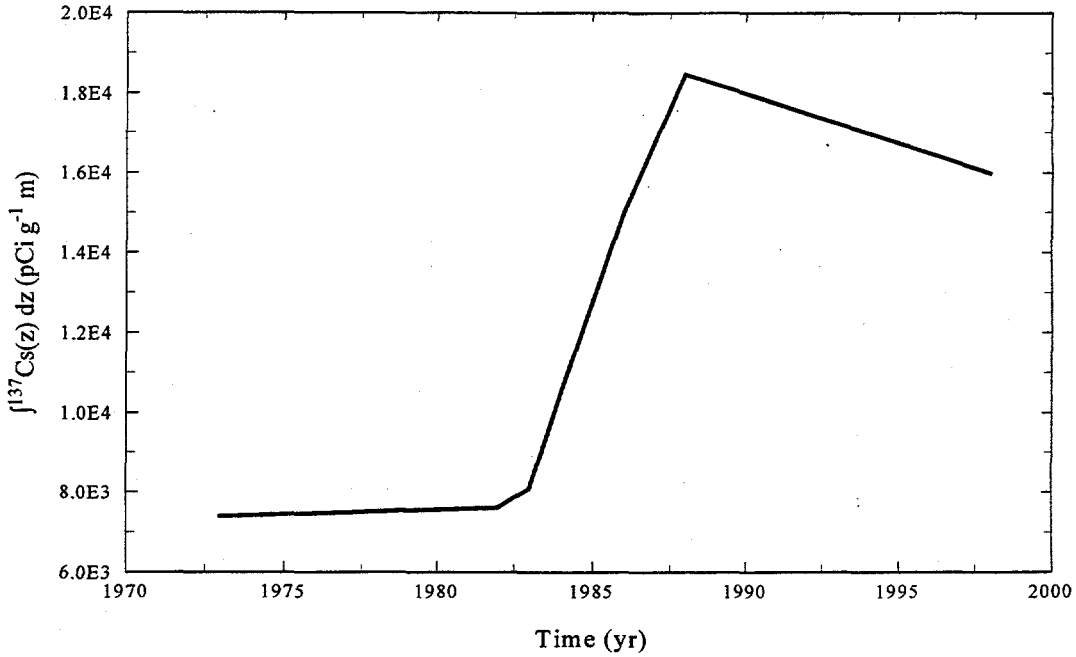

Figure 17. Simulated Accumulation of ^{137}Cs at the Borehole in Response to the Leak History Depicted in Figure 6 and the Conditions Assumed in Case 12 (Figure 16d). Both the Recharge Rate and K_d were Assumed to be Variable.

4.2.1 Comparison With TWRS-EIS Results for ^{137}Cs

There are significant differences between the TWRS-EIS and the STOMP model predictions for the transport of ^{137}Cs to the water table. The TWRS-EIS assumes that ^{137}Cs has a constant K_d of 50 mL g^{-1}. Values of the distribution coefficient of 50 mL g^{-1} and higher are associated with sediment/contaminant interactions associated with typical groundwater chemistry for the Hanford Site. However, much lower values have been found when Hanford sediments interact with ^{137}Cs in high salt solutions (Serne and Burke 1997). With an assumed K_d of 50 mL g^{-1}, calculations showed that ^{137}Cs never arrived at the water table but was instead delayed and decayed to background long before reaching the water table. At 50 mm yr^{-1}, the highest recharge rate assumed by the TWRS-EIS, the peak concentration of ^{137}Cs moved only a fraction of a meter in 30 years and decayed to background in 1000 years, after moving less than 1 m (3 ft.). In contrast, the STOMP modeling reported here incorporates the effect of low and variable K_ds on the movement of ^{137}Cs in the vadose zone. When a the K_d was assumed to be 0 mL g^{-1} and constant for the entire simulation period of 50 yr, ^{137}Cs moved through the vadose zone and arrived at the water table. When an analysis that mimics the observed lithology and the effect of salt concentrations on K_d (Case 12) was performed using STOMP, the resulting ^{137}Cs profile was similar to observations made with spectral-gamma logging in the boreholes adjacent to leaking tanks (GJPO 1996). The peak concentration was located 10 m (32 ft.) below the tank. When the STOMP model incorporated a continuing leak from the tank, the peak concentrations were shown to increase in time similar to that observed in wells adjacent to tank SX-109 (Price 1996). The qualitative features observed by spectral-gamma logging are

captured in the STOMP simulations, which increases confidence in using modeling for predictive assessments in the Hanford tank farms. The simulations clearly identify the impacts of recharge rates, leak volumes, distribution coefficients, and solution density on the migration rates of ^{137}Cs in the vadose zone under the tank farm.

4.3 Transport of ^{99}Tc

While there is some uncertainty about the K_d of ^{137}Cs and how it changes with concentration of competing ions, there is no doubt the K_d of ^{99}Tc is 0 mL g^{-1} in Hanford sediments. The low K_d coupled with a long half-life (2.03×10^5 yr) allows ^{99}Tc to migrate over long distances in both the vadose zone and in groundwater, posing a threat to water quality for a very long time. In this section the distribution of ^{99}Tc in the vadose zone and the flux across the water table are analyzed to determine the impact of specific gravity, stratigraphy, recharge, and leak volume. Note that there is no information on ^{99}Tc distribution in the vadose zone. Therefore, unlike ^{137}Cs, evaluation of the conceptual model is somewhat restricted. In this analysis, all concentrations of ^{99}Tc are expressed in term of pCi L^{-1} in the aqueous phase.

The effect of fluid density on the migration of ^{99}Tc under the assumption of a simple stratigraphy is illustrated in Figure 18. In both cases, plume migration was predominantly vertical in the Hanford Sand unit. The 900 pCi L^{-1} (DWS) isopleth was still well above the water in 1973 when the specific gravity was assumed to be 1.0 (Figure 18a). Lateral spreading was confined to the Early Palouse layer, and there was very little penetration into the coarse Upper Ringold unit. In contrast, the denser fluid was able to overcome the air entry potential of the Upper Ringold unit, resulting in a significant increase in vertical migration and transport across the water table. The major difference between these plumes and the ^{137}Cs plumes at zero K_d is seen in the outer isopleth. Here, the outer isopleth represents the DWS, while in Figure 11 it represents the lower detection limit of the spectral-gamma probe used in borehole logging.

The impact of the amount of stratigraphic detail incorporated into the conceptual model on ^{99}Tc migration is illustrated in Figure 19. Again the plume distribution is somewhat like those observed for non-sorbing ^{137}Cs (Figure 12). The assumption of a simplified stratigraphy resulted in a predominantly vertical movement in the Hanford unit and the borehole was never encountered (Figure 19a). An increased level of stratigraphic detail increased lateral spreading in the Hanford Unit and decreased the rate of vertical migration, and increased lateral spreading. Concentrations exceeded the DWS in the pore water around the entire length of the borehole. Note the movement of the plume along the sloped interface at 30 m (98 ft.). While vertical migration was slowed by the presence of fine and coarse lenses, they did not prevent penetration of the water table (Figure 19b).

There are no data to support any of the simulated distributions of ^{99}Tc in the vadose zone. However, to further evaluate the possible driving forces for transport, the effect of recharge rate was investigated under the complex stratigraphy. The results of the simulations for the year 1983 are summarized in Figure 20.

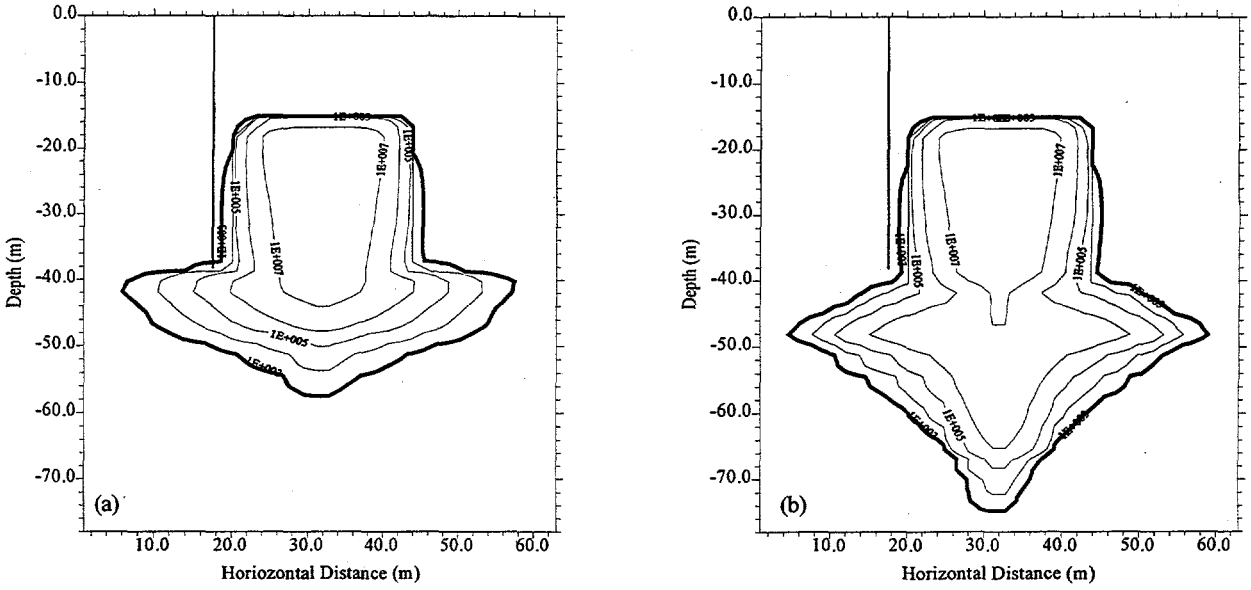

Figure 18. Simulated ^{99}Tc Concentration (pCi L^{-1}) in 1973 Showing the Impact of Specific Gravity on Plume Migration with a Simplified Stratigraphy Under a Variable Recharge (a) Case 1, Pure Water, and (b) Case 3, Specific Gravity =1.4. The vertical line at 17.6 m on the x-axis represents the borehole. The bold isopleth is 900 pCi L^{-1}.

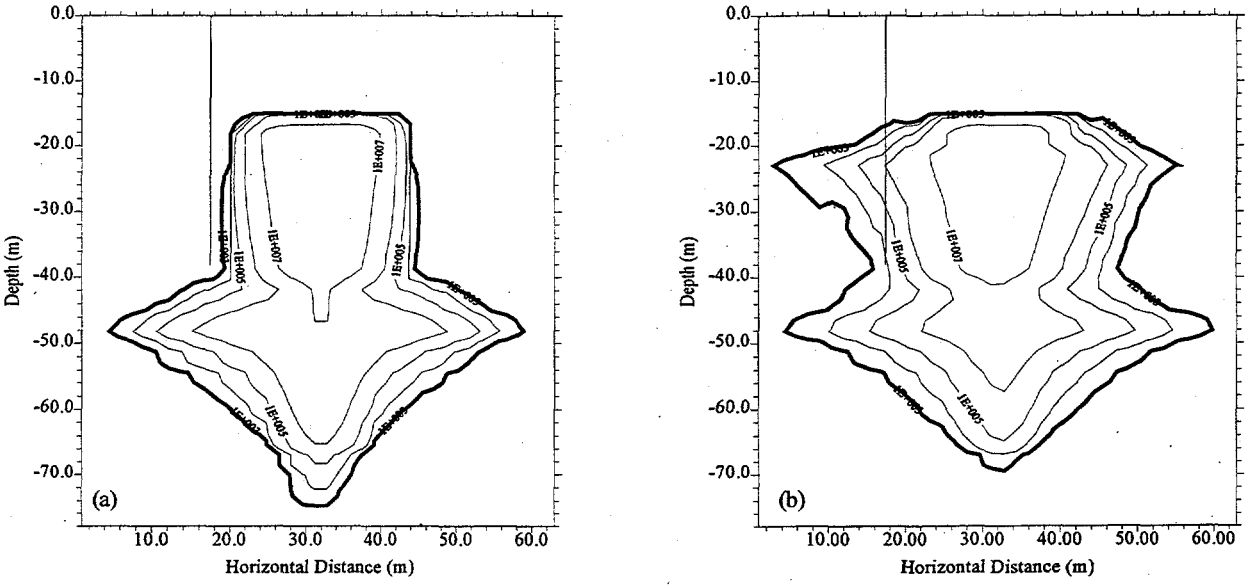

Figure 19. Simulated ^{99}Tc Concentration (pCi L^{-1}) in 1973 Showing the Impact of Stratigraphic Detail on Plume Migration Under a Variable Recharge (a) Case 2, Simple Stratigraphy, and (b) Case 3, Complex. The vertical line at 17.6 m on the x-axis represents the borehole. The bold isopleth is 900 pCi L^{-1}.

As shown in Figure 20a, fixing recharge to 0.5 mm yr^{-1} with a Hanford Barrier limited the depth of penetration of ^{99}Tc to 15 m (49 ft.), even after a 500 m^3 (132,000 gal) leak. When it was assumed that the tank's heat load reduced recharge to 10 mm yr^{-1}, ^{99}Tc was observed to spread throughout the entire simulation domain (Figure 20b). This result is somewhat similar to that with the variable recharge, since it was assumed that the rate was initially equal to 10 mm yr^{-1} increasing in 1983. By the end of 1983, the increase in recharge to 40% of precipitation resulted in a reduction in the lateral extent of the plume as transport became more vertical (Figure 20c). A recharge rate of 100 mm yr^{-1} severely limited the lateral extent of the plume, even in the Early Palouse layer (Figure 20d). At this high recharge rate, the air entry potentials of the capillary breaks were exceeded, removing any impedance to vertical transport. Accurate knowledge of the recharge rate is even more important in predicting the migration of the non-sorbing species such as ^{99}Tc and NO_3^-.

While there are no data to show the distribution of 99Tc in the vadose zone, RCRA monitoring of water wells in the vicinity of WMA-S-SX show evidence of this contaminant in the groundwater. Technetium-99 generally was not measured in groundwater samples before 1986; nevertheless, data from gross beta measurements suggest breakthrough of ^{99}Tc in the second half of the 1980s in the northernmost wells and slightly later in the southern and western wells (Dresel et al. 1996). These data provide a basis for evaluating the conceptual model. The impact of the different components of the conceptual model is best determined by comparing the temporal distribution of the mass flux of ^{99}Tc across the water table. However, the mass flux contains both advective and dispersive components, thereby limiting its application in determining actual concentrations of the contaminant entering the groundwater. To avoid the error involved in converting mass flux to concentration, the time series of ^{99}Tc concentration, averaged over two nodes, at the water table (see Figure 5) were compared. The resulting breakthrough curves for ^{99}Tc are shown in Figure 21, comparing the effects of fluid density, stratigraphy, and recharge rate.

If the density of the leaked fluid is not taken into account, significant error can be introduced into the estimated travel time to the water table (Figure 21a). Taking the DWS of 900 pCi L^{-1} as an indication of the first arrival, ^{99}Tc reached the groundwater in late 1971, and the peak arrived in 1984, when a specific gravity of 1.4 was assumed. In contrast, assuming a specific gravity of 1.0 delayed first arrival until late 1978. By the end of the 50-yr simulation in the year 2015, the peak had not reached the water table. Given the impact of stratigraphy on contaminant migration, these results might be considered a little conservative. The impact of stratigraphy on migration of contaminant plume (specific gravity = 1.4) is illustrated in Figure 21b. With the simplified stratigraphy, the time to first arrival is late 1971, with the peak arriving in 1984. The increased stratigraphic detail resulted in first arrival in 1971, with the peak arriving in 1986. The effect of recharge is illustrated in Figure 21c. For the 50-yr course of the simulation, ^{99}Tc never reached the groundwater under a 0.5 mm yr^{-1} recharge. Under a 10 mm yr^{-1} recharge, the time to first arrival was mid 1971, with the peak arriving in late 1986. The variable recharge boundary condition assumed a fixed rate of 10 mm yr^{-1} until 1983 (Table 4), therefore the time to first arrival was the same as with the 10 mm yr^{-1} rate. The peak also arrived in 1986, although the concentrations were higher. First arrival occurred in mid 1968 under the 100 mm yr^{-1} recharge, and the peak arrived in 1982, although the concentrations were much lower.

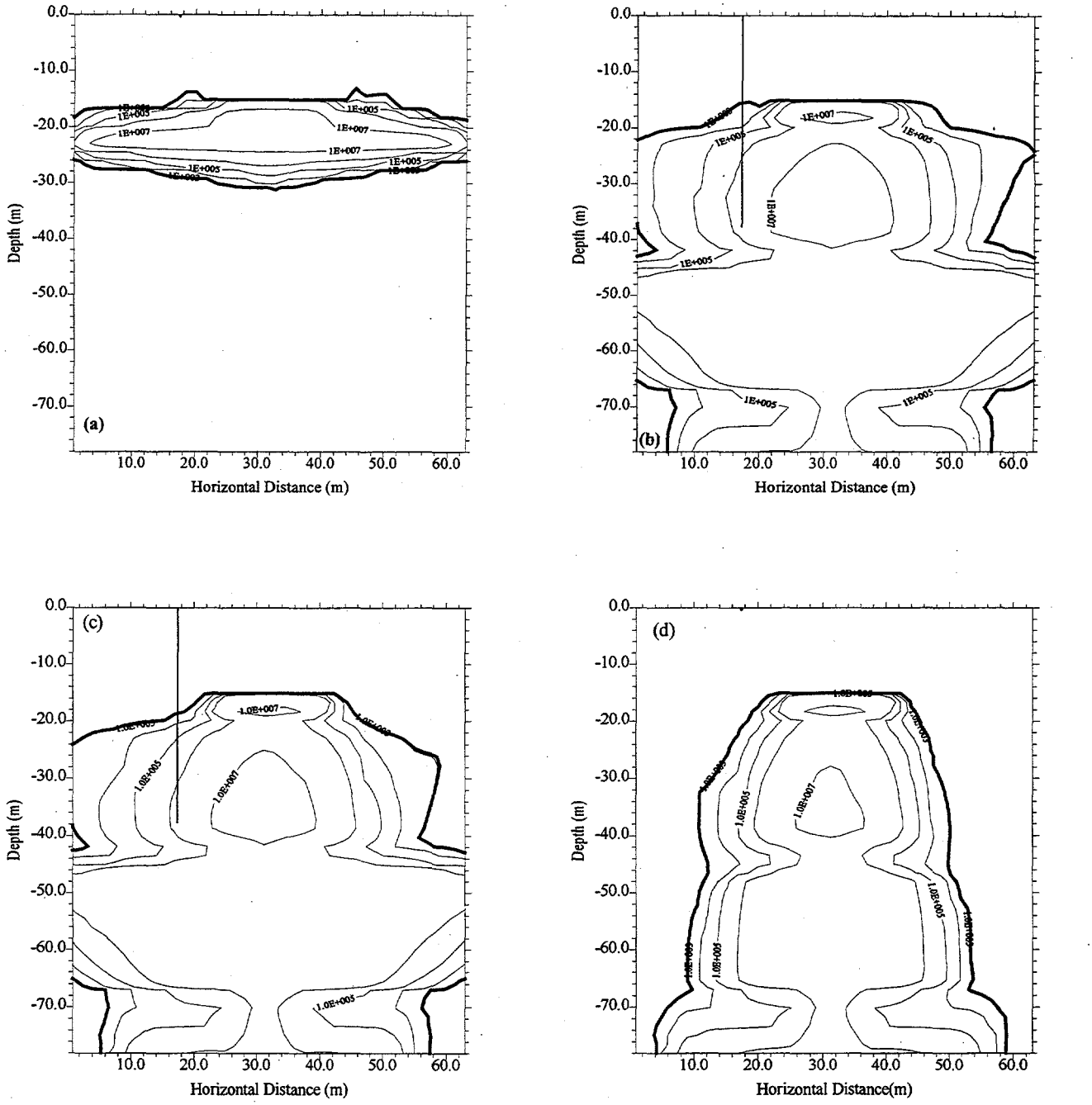

Figure 20. Simulated ^{99}Tc Concentration (pCi L^{-1}) in 1983 Showing the Impact of Recharge Rate , J_w, on Plume Migration (a) Case 4, $J_w = 0.5$ mm yr^{-1}, (b) Case 6, $J_w = 10$ mm yr^{-1}, (c) Case 3, Variable Recharge, and (d) Case 7, $J_w = 100$ mm yr^{-1}. The Vertical Line at 17.6 m on the X-Axis Represents the Borehole. The Bold Isopleth is 900 pCi L^{-1}.

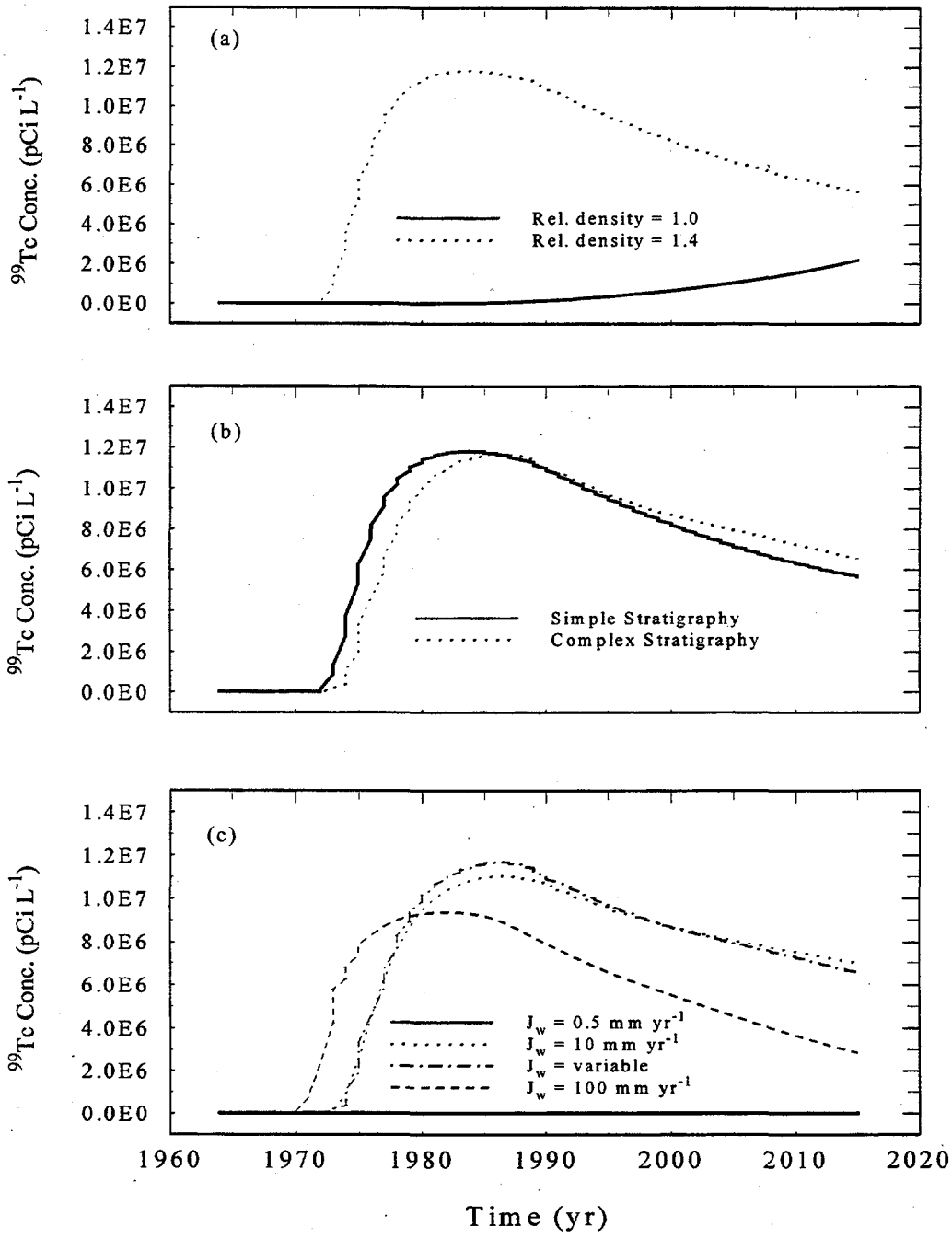

Figure 21. Time Series Plot of Simulated ^{99}TC Concentration (pCi L^{-1}) at the Water Table Below SX-109 Showing the Impact of (a) Specific Gravity, (b) Stratigraphy, and (c) Recharge rate, J_w. In all Cases, a Leak of 500 m^3 (132,000 gal) was Assumed and the Simulations Were Run For 50 yr, Starting in 1964.

The transport of mobile contaminants is dependent on the release history, recharge rate, and stratigraphy, none of which is known with any certainty. The present results are primarily qualitative but they indicate that a leak of 500 m^3 would have resulted in ^{99}Tc reaching the groundwater as early as 1971, with the peak arriving in the mid- to late-1980s. The closest monitoring well to tank SX-109 is 299-W23-39, located approximately 150 m (492 ft.) south, south east of the tank. Concentrations of ^{99}Tc at this well peaked at about 8,000 pCi L^{-1} in 1993 and have been declining since 1994 (Caggiano et al. 1996). The groundwater velocity in the vicinity of WMA-S-SX is between 0.15 m and 0.31 m d^{-1} (0.5 to 1 ft d^{-1}) in a SSE direction. Following the breakthrough of ^{99}Tc at the water table, it would take only 2.5 yr to reach well 299-W22-39. Given the response of well 299-W22-15, concentrations would take about 2 yr to return to background. Thus, a leak of 500 m^3 (1.3 x 10^5 gal) of fluid from tank SX-109 could have resulted in the peak ^{99}Tc concentration reaching the well between 1987 and 1989. The simulated peak concentrations resulting from such a leak are in the range of 1.2 x 10^7 pCi L^{-1}. While these results are not expected to match precisely the field observations at this stage, the high concentrations suggest that either the leak volume or ^{99}Tc inventory may have been overestimated. It could also be a reflection of the conservative, two-dimensional approach used to model a three-dimensional problem. However, given the uncertainty in the input data, the time scales of transport, and the shape of the breakthrough are remarkably similar to field observations. What is also clear is that not all of the ^{99}Tc has been leached from the profile. Thus, additional spikes will likely appear in response to extremes in precipitation.

4.3.1 The Effect of Leak Volume on ^{99}Tc Migration

Under the assumption of a 500-m^3 (132,000 gal) leak, our results show that the groundwater was impacted by mobile contaminants such as ^{99}Tc and NO_3^-. However, the arrival times have been shown to be very sensitive to the release history and leak volume. To evaluate the impact of leak volume and release history, a leak of 15 m^3 (4000 gal) was simulated over a 15-yr period starting in 1964, and compared to previous cases.

Figure 22 compares the impact of specific gravity on the ^{99}Tc breakthrough at the water table. With a specific gravity of 1.0, the first arrival occurred in 2020 (64 yr after the leak started), with the peak occurring in 2123 (159 yr after the leak started).

A specific gravity of 1.4 resulted in a first arrival in 2011 (47 yr after the leak started), while the peak arrived in 2084 (120 yr after the leak started). Table 7 lists the reported travel times for peak and first arrival concentrations for three STOMP cases. Our results for ^{99}Tc appear to match field observations, which showed increased concentrations about 14 yr after the leak, and peak concentrations from 1985 to 1993. While the STOMP calculations are in line with field observations, it is apparent that more detailed measurements of contaminants in the vadose zone will provide a better baseline on which models can be calibrated. A comparison of these results with those for ^{99}Tc in the TWRS-EIS can only be made indirectly since the modeling assumptions are different. However, the results for Case 6 and Case 14 (Table 7) show that travel times are reduced below those predicted for the no-action alternative in the TWRS-EIS. Even when adjustments are made for the start of the leak (the TWRS-EIS no-action alternative assumed the leak to start in 2095, 100 yr after the beginning of the simulation). The shorter travel times is most likely due to the combined effects of leak volume, variable density and recharge rate.

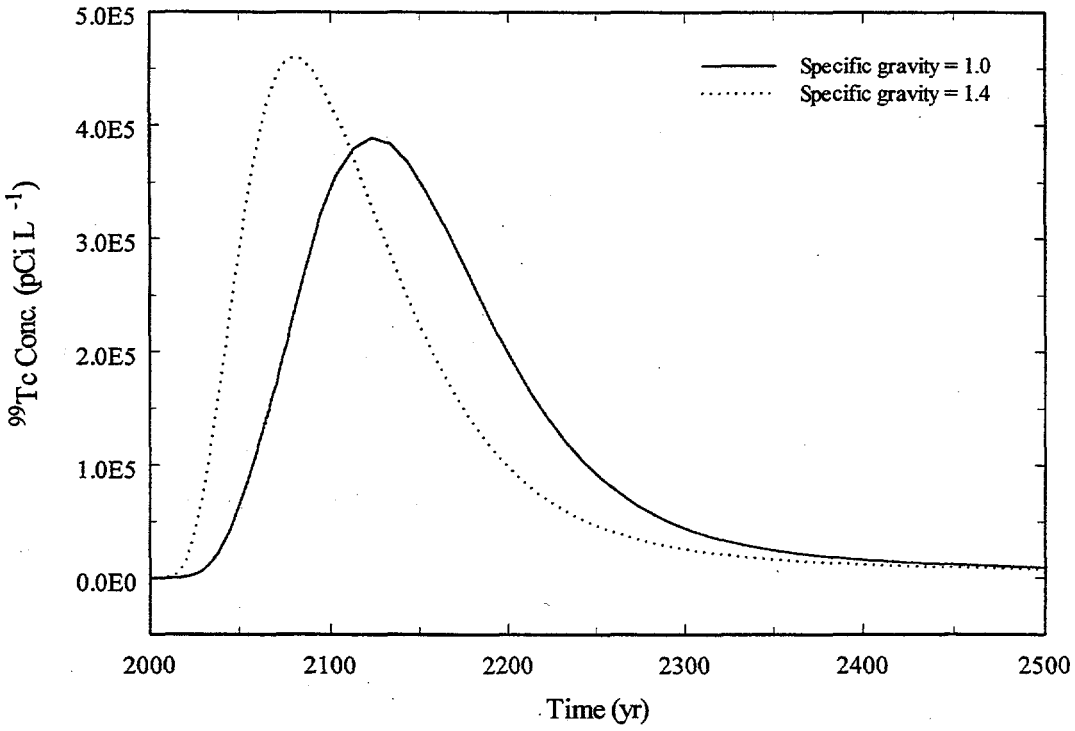

Figure 22. Time Series Plot of Simulated ^{99}Tc Concentration (pCi L^{-1}) at the Water Table Below Tank SX-109 Showing the Impact of Specific Gravity on Plume Migration After a Leak of 15 m^3 (4000) Over a 15-yr Period.

Table 7. Arrival Times at the Water Table for ^{99}Tc (in yr).

Model	First Arrival (yr)	Peak Arrival (yr)
STOMP, Case 13 (variable recharge, Kd = 0 mL g^{-1}, detailed stratigraphy, specific gravity = 1.0, 15 m^3 leak	64	159
STOMP, Case 14 (variable recharge, Kd = 0 mL g^{-1}, detailed stratigraphy, specific gravity = 1.4, 15 m^3 leak	47	120
STOMP, Case 6 (variable recharge, Kd = 0 mL g^{-1}, detailed stratigraphy, specific gravity = 1.4, 500 m^3 leak	7	22

recharge water from rain and snowmelt. This transient water flow around the tank acts to move the contaminants deeper and faster than when one assumes steady recharge rates and one-dimensional flow. Our results for ^{99}Tc appear to match more realistically with observed groundwater monitoring (Caggiano et al. 1996) than with the TWRS-EIS, which predicts first arrival of ^{99}Tc in 150 years and peak concentrations in 260 years. In contrast to the TWRS-EIS predictions, the STOMP simulations predict first arrival at 7 yr and peak concentration at 22 yr. The STOMP estimates of first and peak arrivals are more in line with concentrations measured in downgradient observation wells (Caggiano et al. 1996) for the SX tank farm, which showed increased concentrations about 14 yr after the leak and peak concentrations in wells from 1985 to 1993. While the STOMP calculations are in line with the observations, it is apparent that more detailed measurements of contaminants in the vadose zone will provide a better baseline on which models can be calibrated.

5.0 Conclusions

The primary objective of this study was to examine the relative importance of specific gravity, recharge rate, distribution coefficient, leak volume, and lithology on the spatial distribution of meteoric water and leaked tank fluids in WMA-S-SX. Although the present results are primarily qualitative, they suggest contaminants associated with a leak from tank SX-109 would have impacted the groundwater.

Simulation results show that mechanisms to control recharge would have slowed the advance of the wetting front generated by the leak, and thus any dissolved contaminants. Because of the lower antecedent moisture content, the leaked fluids would have undergone more lateral spreading. All of the simulations show enhanced recharge around the tank perimeters, including the zones in which the boreholes are located. The results of simulations using specific gravities ranging from 1.0 to 1.65 show that the rate of advance of the wet bulb generated by the leaked fluid is sensitive to the fluid density. The rate of advance increases with density because of unfavorable density ratios that cause wetting front instabilities and lead to gravity fingering.

In previous modeling studies, ^{137}Cs was assumed to be immobile with K_ds of 50 to 100 mL g^{-1}. An analysis of data from Raymond and Shdo (1966) suggest that the assumption of such high K_ds may not be valid. A K_d of 0 mL g^{-1} moved the ^{137}Cs unrealistically deep and into the water table, while K_d s of 0.5, 3, and 37 mL g^{-1} kept the ^{137}Cs from arriving at the water table in 50 yr, except under the most extreme conditions (high density and high recharge). When a time-dependent K_d was invoked to mimic the changes that would occur as the concentration of competing ions decreased, the resulting profile provided the best match to field observations. Most of the ^{137}Cs stayed within a 40-m (131-ft.) depth, with the highest concentrations at 20 to 22 m (66 to 72 ft.) below the surface. When small-scale variations in texture were not considered, the mean depth of penetration increase, but the amount of spreading decreased. Controlling recharge had the greatest impact on the extent of plume migration. Even with a K_d of 0 mL g^{-1}, the center of mass of ^{137}Cs remained at 21 m (69 ft.) under a recharge of 0.5 mm yr^{-1}.

Results also show that a leak of 500 m^3 (132,000 gal) of waste would have resulted in the arrival of ^{99}Tc at the groundwater as early as 1971 that peaked in the mid 1980s, with decreased concentrations in the groundwater by 1996. However, by 1996 not all of the ^{99}Tc had been leached from the profile. Within the context of these simulations, there is no doubt that the combination of a long half-life (2×10^5 yr) and a low K_d with a high-density fluid would have resulted in contamination of the groundwater with ^{99}Tc, even without the contribution of flow along well casings, fractures, or clastic dikes. The same conclusion can be drawn about NO_3^-. A breakthrough of NO_3^- in 1971 would have shown up as an increase in bulk electrical conductivity of water samples. Given the uncertainty in the input data, these results compare remarkably well with the data presented by Caggiano et al. (1996). Since the water wells in SX Farm were installed in the early 1990s, there are no data to support the first arrival of mobile contaminants to the water table.

This modeling exercise is by no means exhaustive with respect to the factors than can affect contaminant migration in the Hanford Tank farms. There are many unknowns in modeling contaminant migration in the tank farms. There are also important factors that were not considered in an attempt to simplify the

conceptual model, thus making these results somewhat conservative. Numerical models such as STOMP can provide useful information on tank leak migration and can be used in the evaluation of risk and cost management alternatives. Despite the paucity of information on hydraulic and transport properties, contaminant release histories, leak location, and documentation of water line leaks, this work was able to qualitatively reproduce field observations. However, there is a need for a detailed a geochemical and hydrologic characterization before radionuclide mobility can be modeled adequately.

Success in predicting the migration of contaminants in Hanford's tank farms will require a systematic approach to vadose zone characterization and a thorough analysis and interpretation of existing data.This should include an analysis of breakthrough data for the mobile contaminants, which would permit reconstruction of release histories, a very important step in predictive modeling. It is also clear that vertical borehole monitoring alone cannot provide the quality or quantity of data required for an accurate analysis of contaminant migration in the vadose zone. The inability of the present spectral-gamma logging systems to monitor even a fraction of one percent of the ^{137}Cs inventory will make it difficult to compare results between simulations and measurements except in a qualitative manner. Future characterization activities would be more useful if focused on areas where the early condition was well known such as in the vicinity of tank SX-109, where cores were taken in 1965 shortly after a known leak. The simulated distribution of ^{137}Cs also suggests that a slanted well under a tank would provide invaluable information on the spatial extent of the plume that would be useful in refining the conceptual model. A combination of laboratory studies and field measurements could then be used to develop the proper geochemical relationships for incorporation into an appropriate numerical simulator. It is clear from our simulations that monitoring for gamma emitters, such as ^{137}Cs, to determine their location will provide no information about the mobile contaminants. Future characterization efforts should also consider sampling to determine the distribution of mobile species such as ^{99}Tc and NO_3^- in the vadose zone.

6.0 References

Agnew, S.F. 1996. *Hanford Tank Chemical and Radionuclide Inventories: HDW Model* Rev. 3. LA-UR-96-858. Los Alamos National Laboratory.

Anderson, J. D. 1990. *A History of the 200 Area Tank farms.* WHC-MR-0132. Westinghouse Hanford Company, Richland, Washington.

Aris, R. 1956. "On the dispersion of a solute in a fluid flowing through a tube." *Proceedings of The Royal Society of London Series A,* 235:67-77.

Arnett, R.C., D.J. Brown, and R.G. Baca. 1977. *Hanford Groundwater Transport Estimates for Hypothetical Radioactive Waste Incidents.* ARH-LD-162. Atlantic Ritchfield Hanford Company.

Beck, H. L. 1966. "Environmental Gamma Radiation From Deposited Fission Products 1960-1964." *Health Physics* 12:313-322.

Beven, K. J., D. E. Henderson, and A. D. Reeves. 1993. "Dispersion Parameters for Undisturbed Partially Saturated Soil." *J. Hydrol.* 143:19-43.

Brevick, C. H., L. A. Gaddis, and E. D. Johnson. 1994. *Supporting Document for the Historical Tank Content Estimate for SX Tank Farm.* WHC-SD-WM-ER-324. Westinghouse Hanford Company. Richland, Washington.

Burdine, N. T. 1953. "Relative Permeability Calculations From Pore-Size Distribution Data." *Petrol. Trans. AIME* 198:71-77.

Brooks, R. H., and A. T. Corey. 1966. "Properties of Porous Media Affecting Fluid Flow." *J. Irrig. Drain. Div. Proc. ASCE* 92(IR2): 61-68.

Caggiano, J. A., V. G. Johnson, and C. J. Chou. 1996. *Assessment Groundwater Monitoring Plan for Single Shell Tank Waste Management Area S-SX.* WHC-SD-AP-191 (Rev.0), Westinghouse Hanford Company, Richland, Washington.

Connelly, M. P., B. H. Ford, and J. U. Borghese. 1992. *Hydrogeologic Model for the 200 West Groundwater Area.* WHC-SD-EN-T-014 (Rev. 0), Westinghouse Hanford Company, Richland, Washington.

Dresel, P. E., J. T. Rieger, W. D. Webber, P. D. Thorne, B. M. Gillespie, S. P. Luttrell, S. K. Wurstner, and T. L. Liikala. 1996. *Hanford Site Groundwater Monitoring for 1995.* PNNL-11141. PNL-10285. Pacific Northwest Laboratory, Richland, Washington.

Fauré, M. -H., M. Sardin, and P. Vitorge. 1996. "Transport of Clay Particles and Radioelements in a Salinity Gradient: Experiments and Simulations." *J. Contam. Hydrol.* 21:255-267.

Fayer, M. J., G. W. Gee, M. L. Rockhold, M. D. Freshley, and T. B. Walters. 1996. "Estimating Recharge Rates for a Groundwater Model using a GIS." *J. Environ. Qual.* 25:510-518.

Fayer, M. J., and T. B. Walters. 1995. *Estimated Recharge Rates at the Hanford Site.* PNL-10285. Pacific Northwest Laboratory, Richland, Washington.

Freeman-Pollard, J. R., J. A. Caggiano, S. J. Trent and ENSERCH. 1994. *Engineering Evaluation of the GAO-RCED-89-157, Tank 241-T-106 Vadose Zone Investigation.* BHI-00061. Bechtel Hanford, Inc. Richland, Washington.

Fujikawa, Y., and M. Fukui. 1991. "Analysis of Radioactive Cesium and Cobalt Adsorption to Rocks Using Two-Site Kinetic Model Equations." *J. Contam. Hydrol.* 8:43-69.

Gee, G. W., M. J. Fayer, M. L. Rockhold, and M. D. Campbell. 1992. "Variations in Recharge at the Hanford Site." *Northwest Sci.* 60(4): 237-250.

Gee, G. W., A. L. Ward, B. G. Gilmore, S. O. Link, G. W. Dennis, and T. K. O'Neil. 1996. *Hanford Prototype-Barrier Status Report FY 1996.* PNNL-11367. Pacific Northwest Laboratory, Richland, Washington.

Gee, G. W., D. Rai, and R. J. Serne. 1983. "Mobility of Radionuclides in Soil." pp 203-227. In: D. M. Kral (ed.) *Chemical Mobility and Reactivity in Soil Systems,* SSSA Special Publication Number 11, American Society of Agronomy, Madison, Wisconsin.

GAO. 1989. *Nuclear Waste. DOE's Management of Single-Shell Tanks at Hanford, Washington.* GAO/RCED-89-157. U. S. General Accounting Office, Washington, D.C.

GJPO. 1996. *Vadose Zone Characterization Project at the Hanford Tank farms. SX Tank farm Report.* GJ-HAN-DOE/ID12548-268 (GJPO-HAN-4). U. S. Department of Energy Grand Junction Projects Office, Grand Junction, Colorado.

Hanlon, B.M. 1996. *Waste Tank Summary Report for Month Ending September 30, 1996.* WHC-EP-0182-102. Westinghouse Hanford Company, Richland, Washington.

Hoitink, D. J., and K. W. Burke. 1996. *Climatological Data Summary 1995 With Historical Data.* PNNL-11107, Pacific Northwest Laboratory, Richland, Washington.

Kung, K-J. S. 1989. "Preferential flow in a sandy vadose: 2. Mechanism and implications." *Geoderma,* 46:59-71.

Lindsey, K. A. 1991. *Geologic Setting of the 200 West Area: An Update.* WHC-SD-EN-TI-008. Westinghouse Hanford Company, Richland, Washington.

Low, S. S., W. C. Carlos, J. J. Irwin, R. Khaleel, N .W. Kline, J . D. Ludowise, R. M. Marusich, and P. D. Rittman. 1993. *Engineering Study of Tank Leaks Related to Hydraulic Retrieval of Sludge from Tank 241-C-106.* WHC-SD-WM-ES-218. Rev. 1. Westinghouse Hanford Company, Richland, Washington.

Piepho, M. G. 1994. *Bounding Flow and Transport Analysis of 105A Mock-Up Tank Tracer Test.* WHC-SD-TI-646, Westinghouse Hanford Company, Richland, Washington.

Price, W. H., and K. R. Fecht. 1976. *Geology of the 241-SX Tank farm. ARH-LD-134.* Atlantic Richfield Hanford Company, Richland, Washington.

Price, R. K. 1996. *Evaluation of historical dry well surveillance logs.* WHC-SD-ENV-TI-001. Rev.0. Westinghouse Hanford Company, Richland, Washington.

Raymond, J. R., and E. G. Shdo. 1966. *Characterization of Subsurface Contamination in the SX Tank Farm.* BNWM-CC-701. Battelle Northwest, Richland, Washington.

Relyea, J. F., and R. J. Silva. 1981. *Application of a Site-Binding, Electrical, Double-layer Model to Nuclear Waste Disposal.* PNL-3898. Pacific Northwest Laboratory, Richland, Washington.

Richardson, C.W. 1981. "Stochastic Simulation of Daily Precipitation, Temperature, and Solar Radiation." *Water Resour. Res.* 17:182-190.

Ritchie, J. C., J. R. McHenry, and A. C. Gill. 1972. "The Distribution of ^{137}Cs in the Upper 10 cm of soil Under Different Cover Types in Northern Mississippi." *Health Physics* 22:197-198.

Rockhold, M. L., C. S. Simmons, and M. J. Fayer. 1997. "A Generalized Analytical Solution for One-Dimensional Steady State Infiltration." *Water Resour. Res.* (In Press).

Saiers, J. E. and G. M. Hornberger. 1996. "Migration of ^{137}Cs Through Quartz Sand: Experimental Results and Modeling Approaches." *J. Contam. Hydrol.* 22: 255-270.

Serne, R. J., and D. S. Burke. 1997. *Chemical Information on Tank Supernatants, Cs Adsorption From Tank Liquids Onto Hanford Sediments, and Field Observations of Cs Migration From Past Tank Leaks.* PNNL-11495. Pacific Northwest National Laboratory, Richland, Washington.

Smoot, J. L., J. E. Szecsody, B. Sagar, G. W. Gee, and C. T. Kincaid. 1989. *Simulations of Infiltration of Meteoric Water and Contaminant Plume Movement in the Vadose Zone at Single-Shell Tank 241-T-106 at the Hanford Site.* WHC-EP-0332. Westinghouse Hanford Company, Richland, Washington.

Smoot, J. L., and B. Sagar. 1990. *Three-dimensional Contaminant Plume Dynamics in the Vadose Zone: Simulation of the 241-T-106. Single-Shell Tank Leak at Hanford.* PNL-7221. Pacific Northwest National Laboratory, Richland, Washington.

USDOE. 1996. *Tank waste Remediation system, Hanford Site, Richland, Washington, Final Environmental Impact Statement, Vol. 4.* DOE/EIS-0189. U. S. Department of Energy, Richland, Washington.

Valocchi, A. J. 1985. "Validity of the local equilibrium assumption for modeling sorbing solute through homogeneous soils." *Water Resour. Res.* 21: 808-820.

van Wesenbeeck, I. J., and R. G. Kachanoski. 1994. "Effect of horizon thickness on solute transport." *Soil Sci. Soc. Am. J.* 58:1307-1316.

Ward, A. L., R. G. Kachanoski, A. P. von Bertoldi. 1995. "Field and Undisturbed Column Measurements for Predicting Transport in Unsaturated Layered Soil." *Soil Sci. Soc. Am. J.* 59:52-59.

White, M. D., and M. Oostrom. 1996. *STOMP Subsurface Transport Over Multiple Phases Theory Guide.* PNNL-11217, Pacific Northwest National Laboratory, Richland, Washington.

Wing, N. R., and G. W. Gee. 1994. "Quest for the perfect cap." *Civil. Engr.* 64(10):38-41.

Wood, M. I., R. K. Khaleel, P. D. Rittman, A. H. Lu, S. H. Finfrock, R. J. Serne, and K. J. Cantrell. 1996. *Performance Assessment for the Disposal of Low-Level Waste in the 200 West Area Burial Grounds.* WHC-EP-0645.

Appendix

Method of Moments

Appendix

Method of Moments

The method of moments can be used to determine the transport characteristics of concentration profiles. The moments of a concentration distribution, resulting from a pulse input of solute, can be used to determine the mean and variance from the observed or calculated breakthrough curves (Aris, 1956; Valocchi, 1992). With this approach, it is unnecessary to make assumptions about the nature of the distribution. The n^{th} moment of a concentration distribution with respect to depth (z) is defined as

$$M_n = \int_{-\infty}^{\infty} z^n \, C(z,t)\, dz \qquad \text{(A1)}$$

Equation (4) can be used to calculate the mean travel depth, μ_t, or mean travel time, μ_t, and the variance, σ^2 of the concentration profile, where

$$\mu = \frac{M_1}{M_0} \qquad \text{(A2)}$$

$$\sigma^2 = \frac{M_2}{M_0} - \mu^2 \qquad \text{(A3)}$$

Distribution

No. of Copies

OFFSITE

2 DOE/Office of Scientific and Technical Information

B. Bede
U.S. Ecology
509 E. 12th
Olympia, WA 98501

G. S. Campbell
Washington State University
Geology Department
Pullman, WA 99164

John Conaway
SM-30 Bikini Atol Road
MS J561
Los Alamos, NM 87545

L. G. Everett
Geraghty & Miller, Inc.
3700 State Street, Suite 350
Santa Barbara, CA 93105-3128

S. O. Link
Washington State University
Richland, WA 99352

J. B. Sisson
Lockheed Martin Idaho
P.O. Box 1625
Idaho Falls, ID 83415-5218

R. J. Luxmoore
Oak Ridge National Laboratory
P.O. Box 2008
Oak Ridge, TN 37831

No. of Copies

John Matuszek, PhD
82 McGuffey Lane
Delmar, NY 12054

G. N. Richardson
Hazen and Sawyer
4011 W. Chase Blvd., Suite 500
Raleigh, NC 276073

Dr. John Selker
Bioresource Engineering Dept.
Oregon State University
Corvallis, OR 97331-3906

3 Sandia National Laboratories
P.O. Box 5800
Albuquerque, NM 87185
Attn: S. F. Dwyer
R. E. Finley
S. Webb

B. R. Scanlon
Bureau of Economic Geology
University of Texas at Austin
University Station Box X
Austin, TX 78713-7508

E. Springer
Los Alamos National Laboratory
P.O. Box 1663
Los Alamos, NM 87545

2 Bechtel Nevada
2626 Losee Rd
Las Vegas, NV 89030
Attn: D. G. Levitt
M. J. Sully

No. of Copies

S. W. Tyler
Desert Research Institute
P.O. Box 60220
Reno, NV 89506

2 U.S. Geological Survey
333 W Nye Lane
Carson City, NV 89706
Attn: B. J. Andraski
D. E. Prudic

2 U.S. Nuclear Regulatory Commission
Division of Engineering Safety
Waste Management Branch
11555 Rockville Pike
Rockville, MD 29852
Attn: T. J. Nicholson
E. O'Donnell

W. J. Waugh
Chem Nuclear Geotech
P.O. Box 14000
Grand Junction, CO 81502

S. R. McMullin
U.S. Department of Energy
Savannah River Site
P.O. Box A
Bldg. 703-46A
Aiken, SC 29802

P. J. Wierenga
University of Arizona
Department of Arizona
Department of Soil and Water
429 Shantz Building
Tucson, AZ 85721

Audubon Society of Portland

Diana Bradshaw
Audubon Society of Portland
5151 Northwest Cornell Road
Portland, OR 97210

No. of Copies

Confederated Tribes and Bands of the Yakima Indian Nation

Russell Jim
Environmental Restoration Waste Management Program
P.O. Box 151
Toppenish, WA 98948

Confederated Tribes of the Umatilla Indian Reservation

2 Confederated Tribes of the Umatilla Indian Reservation
P.O. Box 638
Pendleton, OR 97801
Attn: Bill Burke
Tom Gilmore

Columbia Group of Sierra

Carol Lieberman, Chair
Columbia Group of Sierra
2506 Northeast Halsey
Portland, OR 97201

Columbia River United

2 Columbia River United
P.O. Box 912
Bingen, WA 98605
Attn: Greg deBruler
Cindy deBruler

Greenpeace

Charlotte Denniston
Greenpeace
11815 20th Southwest
Seattle, WA 98146

No. of Copies

3 **Hanford Advisory Board**

Max Power
Washington State Department of Ecology
Nuclear Waste Program
P.O. Box 47600
Olympia, WA 98504-7600

Jon Yerxa
U.S. Department of Energy
P.O. Box 550
Richland, WA 99352

Hanford Clearinghouse

Joanne Oleksiak, Director
Hanford Clearinghouse
2829 Southeast Belmont #308
Portland, OR 97214

Hanford Downwinders Coalition

Judith Jurji
Hanford Downwinders Coalition
916 North 36th Street
Seattle, WA 98103

Hanford Downwinders Health Concerns

Lois Camp
Hanford Downwinders Health Concerns
Box 52
Lacrosse, WA 99143

Hanford Education Action League (HEAL)

Lynne Stembridge
Hanford Education Action League
1408 Broadway
Spokane, WA 99201

No. of Copies

Hanford Environmental Dose Reconstruction Project (HEDR)

Greg Combs
Washington State Department of Ecology
Nuclear Waste Program
P.O. Box 47600
Olympia, WA 98504-7600

2 **Hanford Health Effects Subcommittee**

ATSDR Health Council Advisor
ATSDR, MS-E28
1600 Clifton Road N.W.
Atlanta, GA 30333
Attn: Jim Carpenter
Linda A. Carnes

3 **Hanford Health Information Network (HHIN)**

Cindy Green
HHIN Washington State Coordinator
222 West Mission, Suite 122
Spokane, WA 86102

Steve West
HHIN Idaho State Coordinator
Idaho Division of Health
450 West State Street
Boise, ID 83720

Lloyd Athearn
HHIN Oregon State Coordinator
Oregon Health Division
800 NE Oregon Street #21
Portland, OR 97232-0459

No. of Copies

Hanford Thyroid Disease Study

Beth King
Hanford Thyroid Disease Study
MP-425
1124 Columbia Street
Seattle, WA 98104

Heart of America Northwest

Gerald Pollet
Heart of America Northwest, Suite 208
Seattle, WA 98101

Jacobs Engineering Group, Inc.

Phil Rogers
3250 W. Clearwater
Kennewick, WA 99336

2 **Mactec**

Mactec
P.O. Box 1427
Richland, WA 99352
Attn: J. F. Bertsch
J. R. Brodeur

Military Protection Network

Susan Grodon
Military Protection Network
1914 N. 34th Street, #407
Seattle, WA 98103

Natural Resources Defense Council

Natural Resources Defense Council
1350 New York Avenue, Suite 300
Washington, D.C. 20005

No. of Copies

Nez Perce Tribe

Donna Powaukee, Manager
Nez Perce Tribal Department of
Environmental Restoration and Waste
Management
P.O. Box 365
Lapwai, ID 83540

2 **Northwest Environmental Advocates**

Eugene Rosolie
Northwest Environmental Advocates
133 SW 2nd Ave., Suite 302
Portland, OR 97204

Nina Bell, Executive Director
Northwest Environmental Advocates
408 SW 2nd Street, #406
Portland, OR 97214

Northeast Oregon Peace Network

Doug Ray
Northeast Oregon Peach Network
1206 B Avenue
LaGrande, OR 97850

Nuclear Safety Campaign

Bill Mitchell
Nuclear Safety Campaign
1914 North 34th Street #407
Seattle, WA 98103

2 **Oregon Department of Energy (DOE)**

Oregon Department of Energy
625 Marion Street NE
Salem, OR 97310
Attn: Dirk Dunning
David Stewart-Smith

No. of Copies

Oregon Environmental Council

Betty McArtle
Oregon Environmental Council
2637 Southwest Water Avenue
Portland, OR 97201

Oregon Natural Resources Council

James Monteith
1161 Lincoln Street
Eugene, OR 97401

Oregon State Health Division

Ray Paris
Oregon State Health Division
State Office Building
Portland, OR 97204

Oregon State Public Interest Research Group

Sara Laum
Oregon State Public Interest Research Group
027 Southwest Arthur Street
Portland, OR 97201

Oregon Water Resources

Ralph Patt
Water Resources Department
555 13th Street Northeast
Salem, OR 97301

Sierra Club

Frank Hammond
Sierra Club-Cascade Chapter
1516 Melrose Ave.
Seattle, WA 98122

No. of Copies

The Hanford Family

The Hanford Family
1620 Davison Street
Richland, WA 99352
Attn: Mike Fox, President
Cliff Groff

Tri City Industrial Development Council

John Lindsay
Tri City Industry Development Council
901 North Colorado
Kennewick, WA 99336

Umatilla County Commission

Jeanne Hughes
Umatilla County Commission
216 Southeast 4th
Pendleton, OR 97801

4 **U.S. Environmental Protection Agency**

C. E. Findley, Director
U.S. EPA
Hazardous Waste Division (M/C HW-111)
1200 6th Avenue
Seattle, WA 98101

3 U.S. EPA, Region 10
712 Swift Blvd. Suite 5
Richland, WA 99352
Attn: Pam Ennis
Dennis Faulk
Doug Sherwood

U.S. General Accounting Office

Chris Abraham
U.S. General Accounting Office
825 Jadwin Ave. MSIN #A1-80
Richland, WA 99352

No. of Copies

Washington Department of Community, Trade and Economic Development

Mailing Uphouse, Program Coordinator
Washington State Department of Community, Trade and Economic Development
Emergency Management Division
P.O. Box 48346
Olympia, WA 98504

2 **Washington Department of Health**

Joe Jiminez
Washington Department of Health
P.O. Box 47890
Olympia, WA 98504-7890

Kristine Gebbie
Washington Department of Health
1300 Quince
Olympia, WA 98504

Washington Nuclear Waste Advisory Council

Max Power
Washington Nuclear Waste Advisory Council
Washington State Department of Ecology
Mailstop PV-11
Olympia, WA 98504

Washington Physicians for Social Responsibility (WPSR)

Martin Fleck, WPSR
4534 ½ University Way NE
Seattle, WA 98105

No. of Copies

7 **Washington State Department of Ecology**

Jeff Breckel
Washington/Oregon Liason
Washington State Department of Ecology
Mailstop PV-11
Olympia, WA 98504

Scott McKinney
Nuclear Waste Program
P.O. Box 47600
Olympia, WA 98504-7600

5 Washington State Department of Ecology
1315 West 4th Ave.
Kennewick, WA 99336-6018
Attn: Susanne Dahl
Dib Goswami
Moses Jaraysi
Stan Leja
Feng Ma

ONSITE

15 **U.S. Department of Energy Richland Operations Office**

M. J. Furman	H4-83
J. P. Hanson	K8-50
R. D. Hildebrand	H4-83
A. Hon	S7-54
B. Nicoll	S7-53
O. Robertson	H0-12
C. Ruud	S7-54
D. S. Shafer	S7-54
B. Taylor	K6-51
K. M. Thompson	S7-54
D. E. Trader	A5-90
D. M. Wanek	H4-83
D. D. Wodrich	S7-50
W. Wrzesinski	S7-53

DOE-RL Reading Room (1)

No. of Copies		
4	**Bechtel Hanford Incorporated**	
	M. A. Buckmaster	H6-01
	F. M. Corpuz	H4-85
	G. B. Mitchem	H0-17
	C. D. Wittreich	H9-12
8	**Fluor Daniel, Inc. (PHMC)**	
	L. A. Fort	H5-61
	E. A. Fredenburg	H6-12
	C. M. Lewis	R3-25
	F. M. Mann	H0-31
	G. A. Meyer	S2-48
	R. K. Price	N1-55
	A. L. Ramble	T5-54
	R. D. Wojtasek	S7-84

No. of Copies		
44	**Pacific Northwest National Laboratory**	
	C. R. Cole	K9-33
	J. L. Devary	K6-96
	M. J. Fayer	K9-33
	M. D. Freshley	K9-36
	G. W. Gee (10)	K9-33
	D. G. Horton	K6-81
	V. G. Johnson	K6-96
	D. I. Kaplan	K6-81
	R. Khaleel	K5-26
	C. T. Kincaid	K9-33
	R. R. Kirkham	K9-33
	S. P. Lutrell	K6-96
	W. J. Martin	K9-14
	P. D. Meyer	K9-33
	T. L. Page	K9-18
	R. J. Serne	K6-81
	R. M. Smith	K6-96
	M. D. White (3)	K9-33
	A. L. Ward (10)	K9-33
	M. D. Williams	K9-33
	Information Release Office (5)	K1-06